UNIVERSITY OF CALIFORNIA

Santa Barbara

Extreme III-Nitride Alloys Grown via Plasma-Assisted Molecular Beam Epitaxy

A dissertation submitted in partial satisfaction

of the requirements for the degree

Doctor of Philosophy

in

Materials

by

Richard Charles Cramer

Committee in charge:

Professor James Speck, Chair

Professor Claude Weisbuch

Professor Steven DenBaars

Professor Nadir Dagli

September 2019

The dissertation of Richard Charles Cramer is approved.

_____

Professor Claude Weisbuch

_____

Professor Steven DenBaars

_____

Professor Nadir Dagli

_____

Professor James Speck, Committee Chair

August 2019

Extreme III-Nitride Alloys Grown via

Plasma-Assisted Molecular Beam Epitaxy

by

Richard Charles Cramer

ACKNOWLEDGEMENTS

Firstly I would like to thank my advisor Dr. James Speck for his instruction and mentorship throughout my time at UCSB. His assistance with experimental design, data interpretation, lending me books from his personal library, and of course obtaining funding have all been critical for my success in academia. I would also like to thank the rest of my committee Dr. Claude Weisbuch, Dr. Steven DenBaars, and Dr. Nadir Dagli for helping review my research and for assistance at the various academic checkpoints in the last five years.

Within the MBE lab at UCSB there are many to thank. To start off nothing in the MBE lab could be done without the tireless effort of lab managers Kurt Olsson and John English who keep everything up and running. I would also like to thank my MBE mentors Dr. Brian McSkimming, Dr. Erin Kyle, Dr. Erin Young, and Dr. Micha Fireman who taught me how to operate and maintain the MBE; my fellow MBE growers on the Nitride Gen II Kelsey Jorgensen and Christian Wurm; as well as the Nitride 930 growers Christian Bayless, Jianfeng Wang, Kai Shek Qwah, and Morteza Monavarian. Finally I would like to thank the UCSB MBE lab at large for fostering a sense of community, collaboration, and sometimes commiseration.

Beyond the MBE lab I would like to thank Dr. Bastien Boenf for APT analysis of my samples as well as helping co-author two of my publications; Tom Mates for many hours of assistance in the SIMS lab; Dan Cohen for assistance with the transmission spectrometer; the staffs of the XRD lab, AFM lab, and the Nanofab for all they do keeping the facilities available for research any time of the day or night; Chris Zollner for the AlN on SiC

substrates which I used for my BAlN experiments; and the Van de Walle group for their modeling of wurtzite BN, BGaN, and BAlN which was foundational for much of my experimental work.

Outside of the UCSB campus I would like thank my friends, both those in Santa Barbara and those who live elsewhere, who have helped me to stay happy and blow off steam with many game nights, hikes, and beers over the last five years. I would like to thank my parents and my sisters for their constant love and support throughout my many many years of schooling. And finally and most importantly I need to thank my wife Madison Cuneo for moving to Santa Barbara with me and for always supporting my dream to earn a PhD.

To everyone who helped me on this journey,

Thank You

CURRICULUM VITAE OF RICHARD CHARLES CRAMER

August 2019

EDUCATION

University of California Santa Barbara 09/2014 – 09/2019

- PhD Candidate in Materials Science & Engineering, Electronic/Photonic Materials Course Track, GPA 3.62

University of Oregon, Clark Honors College 09/2009 – 07/2014

- B.S. Chemistry, B.S. Physics, Clark Honors College, Cum Laude, GPA 3.77
- U of O Presidential Scholarship, four years tuition, merit-based
- Departmental Honors in Chemistry and Physics, U of O Materials Chemistry Achievement Award

TECHNICAL SKILLS

- *Equipment Maintenance*: Ultra-high vacuum molecular beam epitaxy system including; pumps, gauges, pressure control, gas flow control, high-purity materials handling, respirator training
- *Characterization Techniques*: X-ray diffraction, atomic force microscopy, secondary-ion mass spectroscopy, Hall effect measurements, current-voltage, and capacitance-voltage measurements

EXPERIENCE

Graduate Student Researcher 09/2014 – 09/2019
Lab of Dr. Speck, Materials Department, University of California Santa Barbara

- Operate and maintain a ultra-high vacuum plasma-assisted molecular beam epitaxy (MBE) system
- Develop novel MBE growth techniques for extreme III-nitride alloys such as BGaN, BAlN, and InAlN
- Characterize semiconductor thin films using techniques listed above
- Report findings in technical seminars and peer-reviewed journals: Published three 1st author and one 2nd author paper

Graduate Student Teaching Assistant 01/2017 – 04/2018
Materials Department, University of California Santa Barbara

- Led a group of 6 TA's for a 100+ student undergraduate Materials 101 course
  - Taught the instructional labs for the graduate level an advanced X-ray diffraction methods course

Undergraduate Student Researcher 07/2011 – 07/2014
Lab of Dr. Boettcher, Chemistry Department, University of Oregon

- Assisted in the construction of a novel reactor for the growth of GaAs thin films
- Grew GaAs thin films and characterized photovoltaic properties (I-V & C-V) in a photoelectrochemical cell
- Contributed to two publications in peer-reviewed journals
- Applied and was awarded the $20,000 Beckman Scholarship to fund my undergraduate research

Undergraduate Teaching Assistant 09/2010 – 06/2011
Physics Department, University of Oregon

- Ran teaching labs which accompanied the introductory physics courses for physics majors

PUBLICATIONS

Growth of coherent BGaN films using BBr_3 gas as a boron source in plasma assisted molecular beam epitaxy, **Richard C. Cramer**, Bastien Bonef, John English, Cyrus E. Dreyer, Chris G. Van de Walle, James S. Speck, *Journal of Vacuum Science and Technology A*, **35**, 041509 (2017)

Band gap bowing for high In content InAlN films, **Richard C. Cramer**, Erin E.H. Kyle, and James S. Speck, *Journal of Applied Physics*, **3**, 035702 (2019),

BBr_3 gas as a boron source in plasma-assisted molecular beam epitaxy, **Richard C. Cramer**, Bastien Bonef, and James S. Speck, *Journal of Vacuum Science and Technology A.* In Press (2019)

Nanometer scale composition study of MBE grown BGaN performed by atom probe tomography, Bastien Bonef, **Richard Cramer**, and James Speck, *Journal of Applied Physics*, **121**, 225701 (2017)

Electrochemical Nanostructuring of n-GaAs Photoelectrodes, Andrew J. Ritenour, Solomon Levinrad, Colin Bradly, **Richard C. Cramer**, and Shannon W. Boettcher, *ACS Nano*, **7**, 6840 (2013)

Efficient n-GaAs Photoelectrodes Grown by Close-Spaced Vapor Transport from a Solid Source, Andrew J. Retenour, **Richard C. Cramer**, Solomon Levinrad, and Shannon W. Boettcher, *ACS Applied Materials & Interfaces*, **4**, 69 (2012)

PRESENTATIONS

Growth of BGaN Films Using BBr_3 Gas as a B Source in MBE, **Richard C. Cramer**, Bastien Boenf, and James S. Speck, *13th International Conference on Nitride Semiconductors* Bellevue, Washington, July 7th-12th (2019)

ABSTRACT

Extreme III-Nitride Alloys Grown via Plasma-Assisted Molecular Beam Epitaxy

By

Richard Charles Cramer

Engineering of semiconductor material properties such as band gaps, lattice constants, and polarization charge densities is achieved largely through forming high quality alloys from similar materials. Extreme alloys formed from constituent materials with extreme differences in their base properties enables material property engineering across a larger range of values than traditional alloys. Such extreme alloys represent a scientific opportunity but also a challenge because they are more difficult to grow with high crystal quality than more conventional alloys. This dissertation will present research findings for thin films of the extreme III-nitride alloys InAlN, BGaN, and BAlN grown via the technique of plasma assisted molecular beam epitaxy (MBE).

The InAlN alloy system has band gap energies that span the entire visible range and is a promising candidate for band gap engineering. To facilitate band gap engineering, the band gap bowing for the entire composition range must be well characterized. In rich $In_xAl_{1-x}N$ ($x > 0.60$) films were grown via plasma-assisted MBE on freestanding GaN substrates. The $In_xAl_{1-x}N$ film compositions were determined using high resolution X-ray diffraction (HRXRD). On-axis 0002 omega two-theta scans were used to determine the c spacing of the films, reciprocal space maps of the $\bar{1}015$ peaks were used to determine that the films were completely relaxed, and the film compositions were calculated from that information

assuming Vegard's Law. The band gaps were independently measured using absorbance spectroscopy and fitting to the linear region of a Tauc plot (dependence of α^2 hν on hν) as determined by interpolating the second derivative of the data and selecting a region of low curvature. To compare to literature, the data was fit to a composition-independent band gap bowing model and a bowing parameter of b = 4.0 ± 0.2 eV was calculated, which is consistent with previous results.

Incorporating B into the III-nitride system is predicted to enable higher density polarization charges than is currently possible using AlGaN. However, due to the significant difference between BN and the rest of the III-nitrides, growing high crystal quality films has proven difficult. Additionally B is a difficult material to use in a MBE reactor due to its high melting point as a pure compound and consequently, there is interest in exploring alternative sources for B in MBE.

The construction and operation of a novel BBr_3 gas injection system for a plasma-assisted MBE reactor is detailed. Data from BGaN, BAlN, and hexagonal BN films are presented as a proof of concept for the source and significant additional characterization is presented for the BGaN system. We report the growth of high crystal quality, random alloy $B_xGa_{1-x}N$ thin films with x up to 3.04% and thicknesses up to 280 nm grown on (0001) Ga-face GaN on sapphire. HRXRD was used to measure both the c plane spacing and the strain state of the films. It was determined that the films were fully coherent to the GaN substrate. Elastic stress-strain relations and Vegard's Law were used to calculate the composition. Atom probe tomography (APT) was used to confirm that the $B_xGa_{1-x}N$ films were random alloys. APT and secondary ion mass spectroscopy of a representative $B_{0.03}Ga_{0.97}N$ film showed a high level of Br impurity on the order of 1 x 10^{19}, atoms/cm^3 and atmospheric

contamination consistent with a low purity source. BBr_3 is successful as a B source for high crystal quality BGaN films, however the bromine incorporation from the source limit the applications for BBr_3 as a B source in molecular beam epitaxy.

TABLE OF CONTENTS

Chapter 1: III-nitride alloys

A. Traditional III-nitride alloys

The III-nitride family of semiconducting materials traditionally consists of GaN, AlN, and InN. All are semiconducting, polar, wurtzite phase crystalline materials. The similarity between these materials enables them to be mixed together to form high crystal quality random alloys with a large range of potential properties. For some material properties, such as the lattice constants, the effect of mixing similar materials can be predicted in a simple linear fashion. For example an alloy of $Al_{0.5}Ga_{0.5}N$ has relaxed lattice constants halfway between those of AlN and GaN. This linear relationship is called Vegard's Law and is a very good model for lattice constants and elastic properties of similar alloys.[1] Other material properties such as band gaps and polarization charge densities do not follow such a simple relationship. The dependence of such properties on alloy composition is currently a matter of scientific research. There is significant work being performed by theoretical groups to accurately model and predict alloy properties however many commonly used models consist of empirical fits to experimental data.

The traditional III-nitride alloys have a range of direct band gaps that spans from infrared, 0.7 eV for InN,[2] to ultraviolet to 6.2 eV for AlN.[3] Figure 1.1 shows the band gaps vs a lattice constants[4] for the traditional III-nitride system. The tie lines in Figure 1.1 show the approximate functional form for how the band gap changes with composition for InGaN, AlGaN, and InAlN.[5-7] The deviation from a linear relationship between band gap and composition is called the band bending of the material.

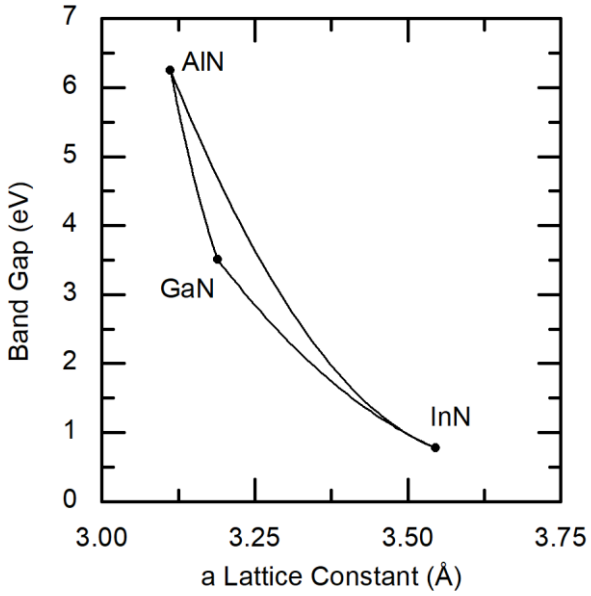

Figure 1.1 Band gaps vs a lattice constants for the traditional III-nitrides
Lattice constants in this system vary linearly with composition (they obey Vegard's Law). The band gaps of the system vary non-linearly with composition. The curved tie-lines drawn are an approximate fit to the band gap vs lattice constant data from the literature.

This variation in band gaps within this materials systems has enabled many III-nitride based technologies to develop. For optical devices (LEDs and lasers) a foundational structure is the quantum well; a region of lower band gap material bordered by regions of higher band gap material. In a quantum well electrons and holes can be localized leading to rapid radiative recombination. For the III-nitride system the most famous example is the work of Shuji Nakamura who used InGaN alloys to make lower band gap active regions in a GaN stack as the foundation of the blue LED for which revolutionized lighting worldwide and won the 2014 Nobel Prize in Physics.[8]

An example of the band structure of a basic quantum well can be seen below in Figure 1.2. The smaller band gap of the InGaN region compared to the surrounding GaN regions localizes electrons and holes in the same physical space which promotes recombination. The electric field in the InGaN QW is due to fixed polarization charges at the InGaN/GaN interfaces due to discontinuities in the total polarization (sum of spontaneous and piezoelectric polarization). Note that for the InGaN layer the piezoelectric polarization is greater than the spontaneous polarization and in the opposite direction which results in the InGaN region having a slant in the opposite sense than the GaN. The Fermi level in this model is the intrinsic Fermi-level which is useful for looking at relative energy values but unlikely to be observed in practice due to unintentional or intentional doping in III-nitrides.

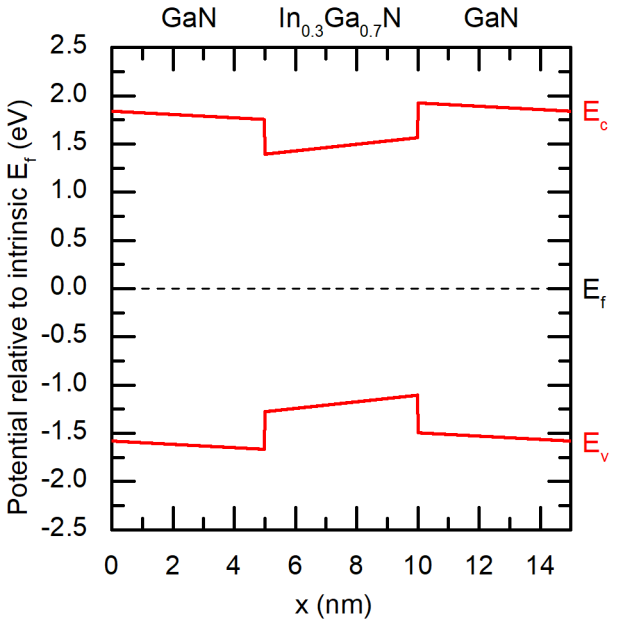

Figure 1.2 Idealized $In_{0.3}Ga_{0.7}N$/GaN quantum well band diagram
An example of the band behavior for a fully strained $In_{0.3}Ga_{0.7}N$ quantum well. The slanted bands are a result of spontaneous polarization in the GaN region and a combination of spontaneous and piezoelectric polarization in the InGaN region. The fermi-level is held at the idealized intrinsic fermi-level since that makes the band gap values easier to read.

The energy (and therefore color) of photons put out by an LED corresponds directly the band gap of the active region which means potentially the III-nitride system could make LEDs of wavelengths from IR to UV.[9] Practically however forming high quality LEDs using an arbitrary III-nitride alloy is non-trivial and this is an area of active research. Recent work has been performed using AlGaN active regions in AlN epitaxial stacks to make UV LEDs which has applications in polymer curing and disinfection.[10-12]

III-nitrides have also had demonstrated uses for lasers.[13] The quantum well is generally a similar stack of quantum wells with additional layers of cladding provided by alloys with a lower index of refraction. The low index of refraction localizes an optical mode which, with

sufficient current, results in stimulated emission in a laser quantum well as opposed to the spontaneous emission of an LED.

The III-nitride alloys form wurzite phase crystals (Fig. 1.3) which have the property of spontaneous polarization in the $[000\bar{1}]$ due to the axial symmetry (point group 6mm). In the modern Berry-phase theory of polarization[14, 15, 16] the polarization in a periodic crystal is a multivalued vector quantity which can be qualitatively thought of as the set of all potential sums of dipoles in the crystal. Due to the lack of a unique origin in a crystal there is not a unique solution for the value of polarization. Instead the polarization is multivalued; an infinite set of solutions depending on how the boarders of the problem are defined. However due to the periodicity of the crystal the set of solutions is quantized in a way that makes it tractable. Experimentally the polarization values that are measured are always relative to a non-polar reference state such that they are single valued differences in the multivalued polarization quantities. For the III-nitrides the spontaneous polarization is rigorously defined as the difference between the multivalued polarizations of the relaxed polar material and a strained non-polar state.

Polarization is fundamentally a result of the geometry of the crystal and can be greatly influenced by deformation of the crystal lattice. This strain induced polarization is called the piezoelectric polarization. For the III-nitride system compressive strain such as InGaN strained to GaN results in piezoelectric polarization in the [0001] direction while tensile strain, such as AlGaN strained to GaN results in piezoelectric polarization in the $[000\bar{1}]$. For stained layers the resultant polarization is always a combination of the spontaneous and piezoelectric polarization effects.

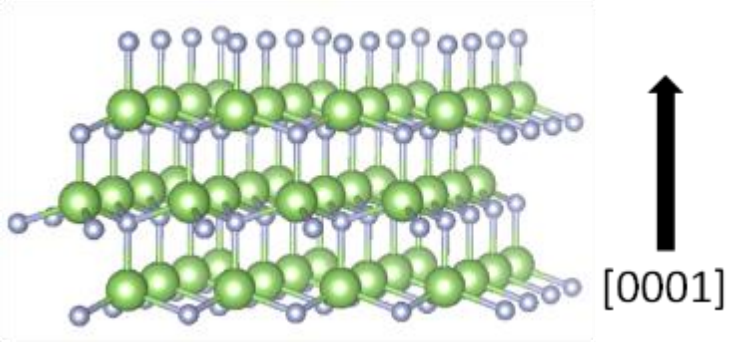

Figure 1.3 Wurtzite crystal structure of GaN
Gallium atoms are green, nitrogen atoms are blue. The normal growth direction for III-nitrides is in the [0001] direction shown by the arrow. For the III-nitrides there is a spontaneous polarization in the $[000\bar{1}]$ direction (antiparallel to the arrow).

The (0001) c plane is the most common growth plane for the III-nitrides. However the polarization in the III-nitride system leads to a vertical polarization field in c-plane III-nitride devices. This field is detrimental to c-plane LEDs since the presence of the polarization field localized holes and electrons to opposite sides of the quantum wells, this is known as the quantum-confined stark effect.[17] Note that in Figure 1.2 the quantum well InGaN section has an electric field that drives electrons to the left side of the well and holes to the right. This effect is the motivation for significant research in growing III-nitride LEDs in geometrics other non-polar and semi-polar planes.[18]

The polarization of the III-nitride system has practical applications in the formation of two dimensional electron gasses (2DEGs). At the junction of two layers of materials with dissimilar polarization (such as two different III-nitride alloys) there is a discontinuity in the polarization filed which leads to a localized charge at the interface. In many practical applications the discontinuity is due to a combination of both intrinsic and piezoelectric

polarization.[19, 20] The presence of a localized sheet of positive charge at one side of the interface due to polarization results in the accumulation of electrons on the other side of the interface. These accumulated electrons form a 2DEG where they have high mobility. AlGaN on GaN and lattice matched $In_{0.18}Al_{0.82}N$ on GaN interfaces have been used to make world record mobility high electron mobility transistors (HEMTS).[21] An extremely basic HEMT structure using AlGaN on GaN is shown below in Figure 1.4, the 2DEG formed by the polarization discontinuity between the AlGaN and the GaN creates a highly conductive region which connects the source and the drain. This region can be pinched off by applying voltage to the gate creating a basic transistor.

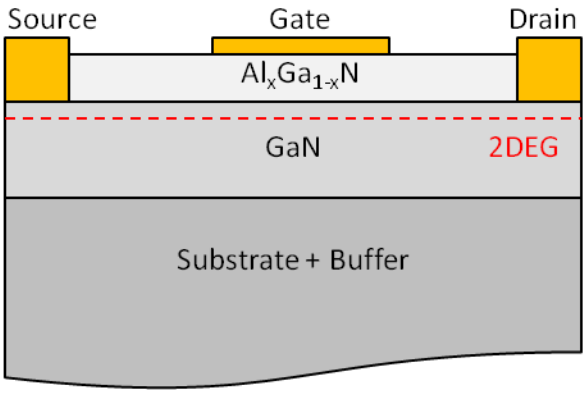

Figure 1.4 Basic AlGaN/GaN HEMT structure
The above diagram is one of the simplest forms for an AlGaN/GaN HEMT. In this normally on transistor design the 2DEG formed at the AlGaN GaN interface provides a high mobility channel between the source and the drain which can be pinched off by applying a voltage to the gate. Modern HEMTs have additional features to optimize performance such as passivation layers, field plates, and n^+ doped contact regions for the source and drain.

In addition to the potential for high electron mobility GaN based electronics are useful due to the large band gap of GaN. The larger band gap (compared to Si) makes GaN capable of holding larger voltage loads before breakdown. Combining high mobility and high voltage makes GaN a material of choice for many high power devices. GaN is an attractive material for high frequency power transistors due to its large breakdown electric field (3.3 MV cm^{-1}) and high saturation electron velocity ($2.5x10^7$ cm s^{-1}), this result in GaN having a higher Johnson's figure of merit that Si, GaAs, and InP.[22, 23]

B. Growth of III-nitrides

The growth of epitaxial layers for III-nitride devices is largely limited by the choice of substrate. Homoepitaxial growth is generally higher quality than heteroepitaxy and therefore having GaN or AlN substrates would be ideal for many devices. Unfortunately bulk GaN growth and bulk AlN growth are immature technologies. Growth is slow and boule size is measured in centimeters, compared to the Si industries meter sized boules. This lack of economy of scale keeps freestanding GaN and AlN substrate prices high. Additionally the crystal quality is not as high as Si and freestanding GaN substrates have threading dislocation densities on the order of 10^6 cm^{-2} despite this they are still the best substrates for many III-nitride devices.[24]

Sapphire has a lattice mismatch of 15% with GaN which leads to a threading dislocation density on order 10^8 cm^{-2} in the GaN buffer layer.[25] During growth of the initial GaN layer nucleation occurs at several points on the sapphire substrate and these islands grow and coalesce into a film, due to the lattice mismatch when these islands meet they do not merge into a continuous film but form vertical lattice defects. These vertical defects propagate along the growth direction (usually [0001]) and continue into all subsequently deposited layers. These threading dislocations serve as leakage pathways and nonradiative recombination centers which is detrimental many devices.[26]

Other substrates which are used for III-nitride epitaxy are Si (111) and SiC. Si (111) is attractive because of its high crystal quality and low cost but suffers from a large lattice mismatch which results in poor epitaxy. SiC has a closer lattice match than sapphire but suffers from poor surface wetting which also results in poor epitaxy. Sapphire represents an

intermediate cost and quality and is the most commonly used substrate for GaN, though freestanding GaN is the best if budget allows.

The most common industrial method for growing epitaxial III-nitride films is metal-organic chemical vapor deposition (MOCVD) which is a chemical process where precursor gases react at a substrate surface to leave a III-nitride film on the surface. Commonly the nitrogen is provided by ammonia and the group III metal is provided by a trimethyl or triethyl organometallic gas. Organometallic precursors are expensive and the gases are highly toxic however high growth rate and good crystal quality have made this the industry standard.[27]

Molecular Beam Epitaxy (MBE) has been used to make higher crystal quality III-nitride films than MOCVD. While the growth rate is substantially slower the ability to perform in-situ characterization via reflection high energy electron diffraction (RHEED), and the lower growth pressures allows for higher overall crystal film quality at the expense of growth rate.

The general principle of MBE is to supply only the needed reagents to grow the crystal. The MBE chamber is kept in ultra-high vacuum and the reagents are added in the simplest form possible. For metals such as Ga, Al, In, Si, and Mg pure metals are placed in high temperature crucibles (either pyrolized boron nitride or graphite) and a small flux of atoms is vaporized or sublimated off of the pure sample. In the vacuum environment of the MBE the vaporized atoms have no inter-atom interactions on the length scale of the chamber and to a good approximation follow a simple liner trajectory and are thus molecular beams (or quite commonly, atomic beams.

There are two distinct methods of MBE growth for III-nitrides defined by how the nitrogen is introduced. Plasma-assisted MBE flows nitrogen gas though a radio frequency

plasma cavity which converts 1-5% of the gas into reactive atomic N which can incorporate into the growing film.[28] Recent work out of UCSB demonstrates that using a high flux nitrogen plasma it is possible to obtain growth rates of 7.6 um/hr.[29] This high growth rate has the potential to make MBE competitive with MOCVD in terms of growth rate for III-nitrides. Ammonia MBE uses NH_3 gas instead of N_2 which is reactive enough to crack on a hot substrate surface to form N (which incorporates into the crystal) and H/H_2 which also incorporates into the crystal but at a relatively low rate. In this document we will discuss III-nitride alloys grown using the method of plasma assisted MBE.

A schematic of the Nitride Gen II MBE system at UCSB which was used for all experiments presented in this document is shown in Figure 1.5. The growth chamber is kept in vacuum 10^{-10} Torr at idle and 10^{-5} Torr during growth (of which nearly all of the pressure is due to unreactive N_2). Pure metal sources of group IIIs (Ga, In, and Al) are positioned in upward facing ports where they are melted then vaporized to form atomic molecular beams. Doping sources Mg, and Si are positioned in downward facing ports where they are sublimated from a solid source to form a molecular beam. The central viewport serves as a way to measure substrate temperature via infrared pyrometry as well as an injection tube for other gas sources. The substrate is positioned on a central continuous azimuthal rotation (CAR) system which can be rotated 180° such that an ion gauge can be moved into the substrate position. This ion gauge is used to measure beam equivalent flux's in qualitative units of Torr from the sources. Finally the reflection high-energy electron diffraction (RHEED) setup consists of an electron source on one side of the system lined up with the substrate position and a phosphor screen on the opposite side. Electrons provided by the RHEED source hit the substrate at a very low angle and diffract with the surface, the

resulting diffraction pattern can be easily observed on the phosphor screen where the diffracted electrons cause the phosphors to luminesce.

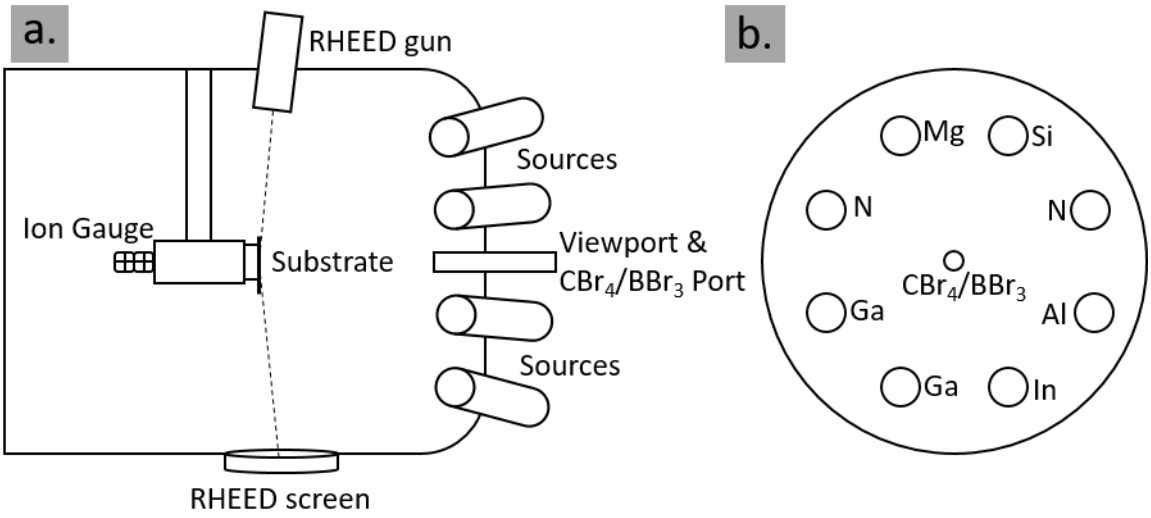

Figure 1.5 Schematic of a molecular beam epitaxy system
(a.) Side view of the system (b.) Front view of the system. The source positions are labeled as they were in 2019 on the "nitride" Varian Gen II MBE system at UCSB.

Some elements cannot be easily vaporized from an atomic source. On the Nitride Gen II system we use two such elements B and C. It has been demonstrated that C doping of nitrides can be achieved by flowing CBr_4 gas into the chamber, the C incorporates into the film while the Br does not.[30] Similarly in this dissertation we will present information on the use of BBr_3 as a gas source for B in MBE. On the Nitride Gen II system both are injected through the gas injection line around the central viewport.

C. High resolution X-ray diffraction

High Resolution X-ray diffraction (HRXRD) is one of the most useful methods for characterizing crystalline films and has been extensively studied for the III-nitride system.[31] When analyzing the data from an HRXRD experiment it is useful to contextualize the results in terms of reciprocal space. Reciprocal space is a model where real space has been inverted via a Fourier transform. What is big becomes small, what is small becomes big, and near-infinitely repeating planes such as those found in a perfect crystal are transformed into near-points of intensity. For the specific sets of experiments discussed in this document two reflections are of particular importance 0002 and $\bar{1}015$. A reciprocal space diagram showing the positions in reciprocal space for those reflections of InN, AlN, and GaN are shown in Figure 1.6.

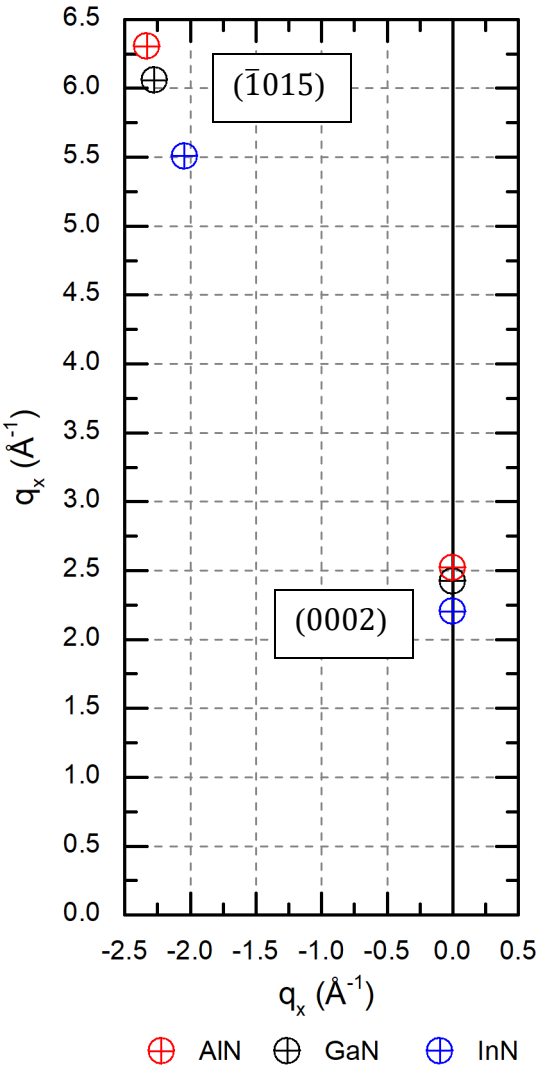

Figure 1.6 Reciprocal space map of HRXRD peaks commonly used for III-nitrides The 0002 on-axis peaks gives information about the c parameter of the film and, if thickness fringes are present, the thickness of the coherent region. The off axis $\bar{1}015$ peaks give information about both the a and c parameters of the film.

The 0002 point in reciprocal space is the reflection caused by the 0002 planes within the crystal. In practice this is measured using an ω-2θ scan which measures a line in reciprocal space somewhere along q_x =0. As can be seen in the diagram the different points along this line in reciprocal space correspond to different materials as determined by their c parameters. For III-nitrides the position in reciprocal space of 0002 peak is

$$q_x = 0 \;\; q_y = (2)\frac{2\pi}{c} \tag{1.1}$$

where c is the lattice parameter of the crystal. It is important to note the HRXRD measures the sample crystal directly so if there is a strain effect that modifies the c parameter of the crystal than the HRXRD point will likewise shift. HRXRD will only measure lattice constants if the film is fully relaxed. In addition to giving the c spacing of the film the 0002 reflection is also useful for determining the thickness of a film. In reciprocal space the breadth of real space in which a set of planes is coherent will be transformed into a Sinc function around the central peak intensity. If the film is of sufficient structural quality this will result in easily observed fringes of Laue oscillations. These are a result of interference between diffracted beam paths at the interfaces. As this is a secondary effect it is only observed when there is a coherent region to diffract from and is therefore an indicator of coherence length which in a good crystal correlates directly with thickness.

The other important reflection used in this work is the $\bar{1}015$ reflection. This corresponds to a point in reciprocal space where

$$q_x = (-1)\frac{4\pi}{a\sqrt{3}} \;\; q_y = (5)\frac{2\pi}{c} \tag{1.2}$$

c and a are the lattice parameters of the film. If the film is strained c and a are the strained lattice parameters. Measuring this point experimentally is more different as it is impossible to obtain all the information from the point in a single line scan so instead we generally perform a 2D measurement of reciprocal space around the point known as a reciprocal space map. Determining the relative positions of a film peak compared to a substrate peak can help determine the strain state of a film. If the substrate and film peak have the same q_x value that corresponds to the films having the same a parameter and thus the film is fully coherent to with the substrate. Conversely if the film and substrate have different q_x values than you know that the film is at least partially relaxed.

D. Extreme alloy research

Much of the work on traditional III-nitrides is focused on compositions which are nearly lattice matched to an available substrate. Examples include as Al-rich alloys on AlN, Ga rich alloys on GaN, or InAlN close to 18% In which is lattice matched with GaN. This is a practical limitation for research focused primarily on forming devices. In this dissertation we will focus on "extreme III-nitride alloys" meaning alloys of III-nitrides that are formed from the more disparate constituent materials.

In Chapter 2 of this dissertation we will examine some of the challenges in growing and characterizing high In content InAlN films. In Chapters 3, 4, and 5 we will focus on incorporating the group III element B into the III-nitride family using a novel BBr_3 B source developed at UCSB.

BGaN and BAlN alloys are difficult to grow due the extreme differences in the material properties. BN is most stable in a hexagonal layered crystal structure (Figure 1.4) as opposed to the wurtzite crystal structure formed by the other III-nitrides (Figure 1.2). Additionally B is significantly smaller than other group III elements and is particularly difficult to use in MBE which motivated the construction of a novel gas source.

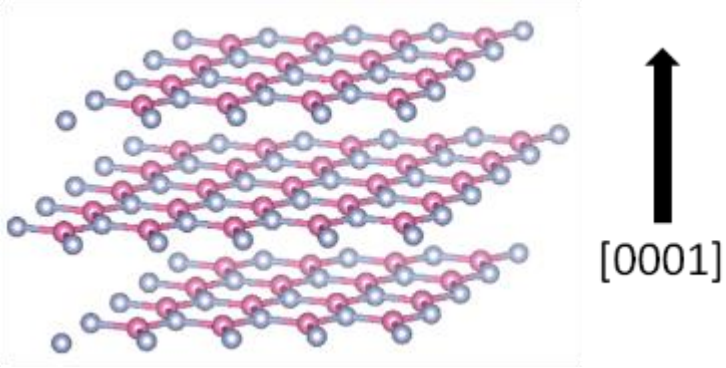

Figure 1.7 Layered hexagonal structure of BN
Pink sheres are B, gray-blue spheres are N.

BGaN and BAlN alloys have potentially useful properties for expanding the III-nitride system. It has been predicted that BGaN and BAlN alloys may have high polarization charge densities with GaN interfaces making them potentially useful for HEMT technologies.[32] Additionally if is predicted that incorporating B would expand the space of potential band gaps in the III-nitride system even further. Figure 1.4 shows a band gap vs lattice constant plot for the III-nitrides system including theoretical values for wurtzite phase BN.[33] Wurtzite phase BN is unstable but it is the proper reference point for predicting the properties of wurtzite phase BGaN and BAlN alloys. There is an additional complication for band gaps in that wurtzite phase BN is predicted to have an indirect band gap so at some point there will be a transition from the direct $\Gamma \rightarrow \Gamma$ type transition of the traditional group III-nitrides to an indirect $\Gamma \rightarrow X$.[34]

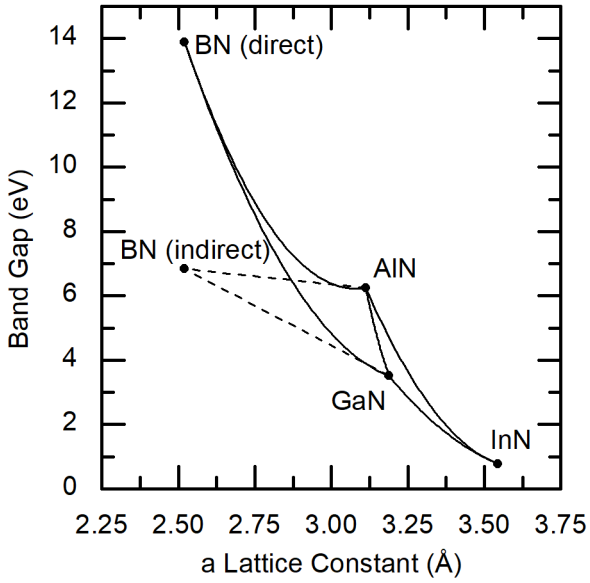

Figure 1.8 Band gaps vs a lattice constants for the expanded III-nitride system
The AlN, GaN, and InN band gaps vs compositions are the same as in Figure 1.1 the theoretical values for wurtzite BN expand the system further though it is unlikely that high B composition alloys would remain in the wurtzite phase. Note that for wurtzite phase BN the direct $\Gamma \rightarrow \Gamma$ band gap is larger than the indirect $\Gamma \rightarrow X$ band gap. At some B composition there would be a direct to indirect band gap transition. The tie lines from AlN and GaN to BN are predications with a low degree of confidence.

The band gaps of the traditional III-nitrides (AlN, GaN, and InN) spans the entire visible range (~1.7 eV to ~ 3 eV). Adding in theoretical values for wurtzite phase BN expands this range though high B concentration alloys may not be stable. Solid lines show approximate deviations from Vegard's Law with composition. At some B concentration the band gap would be indirect rather than direct.

Chapter 1 References

[1] L. Vegard, Zeitschriftfür, Physik 5, 17 (1921).

[2] J. Wu, W. Walukiewicz, W. Shan, K.M. Yu, J.W. Ager III, S.X. Li, E.E. Haller, H. Lu, and W.J. Schaff, J. Appl. Phys. 94, 4457 (2003).

[3] L. Chen, B.J. Skromme, R.F. Dalmau, R. Schlesser, Z. Sitar, C. Chen, W. Sun, J. Yang, M.A. Khan, M.L. Nakarmi, J.Y. Lin, and H.X. Jiang, Appl. Phys. Lett. 85, 4334 (2004).

[4] I. Vurgaftman, and J.R. Meyer, J. Appl. Phys. 94, 3675 (2003).

[5] R.C. Cramer, E.C. Kyle, and J.S. Speck, Journal of Applied Physics Vol, Page, 2019

[6] B.S. Eller, J.L. Yang, R.J. Nemanich, J. of Elec. Mat. 43¸ 4560 (2014)

[7] J. Wu, W. Walukiewicz, K.M. Yu, J.W. Ager, E.E. Haller, H. Lu, W.J. Schaff App. Phys. Lett. 80 4741 (2002)

[8] S. Nakamura, Rev. Mod. Phys. 87, 1139 (2015)

[9] J. Wu, J. Appl. Phys. 106 1011101 (2009)

[10] D.B. Li, K. Jiang, X. J. Sun, C.L. Guo, Adv. Opt. Photonics 10, 43, (2018)

[11] M.S. Shur, R. Gaska, IEEE Trans. on Elec. Dev. 57, 1, (2010)

[12] M. Kneissl, T. Kolbe, C. Chua, V. Kueller, N. Lobo, J. Stellmach, A. Knauer, H. Rodriguez, S. Einfeldt, Z. Yang, N.M. Johnson, and M. Weyers Smicond. Sci. Technol. 26, 014036 (2011)

[13] Y. Sun, K. Zhou, Q. Sun, J. Liu, M. Feng, Z. Li, Yu. Zhou, L. Zhang, D. Li, S. Zhang, M. Ikeda, S. Liu, H. Yang, Nature Photonics 1, 595 (2016)

[14] R. Resta and D. Vanderbilt, in *Physics of Ferroelectrics: A Modern Perspective* (Springer, Heidelberg, 2007), pp. 31-68

[15] F. Berdardi, V. Fiorentini, and D. Vanderbilt, Phys. Rev. B 56, R10 024 (1997)

[16] R.D. King-Smith and D. Vanderbilt, Phys Rev. B 47, 1651 (1993)

[17] N. Grandjean, J. Massies, M. Leroux, M. Laugt, P. Lefebvre, B. Gil, J. Allegre, P. Pigenwald MRS Interned J. Nitride Semicond. Res. 4 G11.7 (1999)

[18] H. Masui, S. Nakamura, S. P. DenBaars, U. K. Mishra, IEEE Trans. on Elec. Dev. 57 88 (2010)

[19] C. E. Dreyer, A. Janotti, C. G. Van de Walle, D. Vanderbilt Phys. Rev. X 6, 021038 (2016)

[20] K. Liu, H. Sun, F. AlQatari, W. Guo, X. Liu, J. Li App. Phys. Lett. 111 222106 (2017)

[21] E.C.H. Kyle, S.W. Kaun, P.G. Burke, F. Wu, Y.R. Wu, J.S. Speck J App. Phys 115 193702 (2014)

[22] Stephen Kaun, Man Hoi Wong, Umesh K Mishra, Semicond. Sci. Technol. 28 074001 (2013)

[23] Mishra U K, Shen L., Kaxior T E and Wu Y-F, proc. IEEE 96 287

[24] E. C. H. Kyle, S. W. Kaun, P. G. Nurke, F. Wu, Y. R. Wu, J. S. Speck. J. App. Phy. 115 193702 (2014)

[25] L. Liu, J.H. Edgar. Mat Sci and Enge R 37 2002, 61-127

[26] J. S. Speck, S. J. Rosner, Physica B: Cond. Matte, 15, 273-274 (1999)

[27] I. M. Watson, Coordination Chemistry Reviews 257 2120-2141 (2013)

[28] S. Agarwal, B. Hoex, M.C.M. Van de Sanden, D. Maroudas, E.S. Aydil, Appl. Phys. Lett. 83, 4918 (2003)

[29] B. McSkimming, C. Chaix, J. S. Speck, J. Vac. Sci. Technol. A 33 05E128 (2015)

[30] D.S. Green, U.K. Mishra, and J.S. Speck, J. Appl. Phys. 95, 8456 (2004).

[31] M.A. Moram, M.E. Vickers, Rep. Prog. Phys. 72 036502 (2009)

[32] L. Kikai, H. Sun, F. AlQatari, W. Guo, X. Liu, J. Li, C.G. Torres Castanedo, X. Li, Appl. Phys. Let. 111, 222106 (0217)

[33] C.E. Dreyer, J.L. Lyons, A. Janotti, C.G. Van de Walle, Appl. Phys. Lett. 7, 031001 (2014)

[34] J.X. Shen, D. Wickramarantne, C.G. Van de Walle, Phys. Rev. Materials 1, 065001 (2017)

Chapter 2: Band gap bowing for high In content InAlN films

The InAlN alloy system is an example of an extreme III-nitride alloy additionally the system has band gap energies that span the entire visible range and is a promising candidate for band gap engineering. To facilitate bandgap engineering, the bandgap bowing for the entire composition range must be well characterized. In rich $In_xAl_{1-x}N$ ($x > 0.60$) films were grown via plasma assisted molecular beam epitaxy on freestanding GaN substrates. The $In_xAl_{1-x}N$ film compositions were determined using high resolution X-ray diffraction. On-axis 0002 omega two-theta scans were used to determine the c spacing of the films, reciprocal space maps of the $\bar{1}015$ peaks were used to determined that the films were completely relaxed, and the film compositions were calculated from that information assuming Vegard's Law. The band gaps were independently measured using absorbance spectroscopy and fitting to the linear region of a Tauc plot (dependence of α^2 hν on hν) as determined by interpolating the second derivative of the data and selecting a region of low curvature. To compare to literature the data was fit to a composition-independent band gap bowing model and a bowing parameter of $b = 4.0 \pm 0.2$ eV was calculated which is consistent with previous results. This work is reprinted with permission from the Journal of Applied Physics [Band gap bowing for high In content InAlN films, Richard C. Cramer, Erin E.H. Kyle, and James S. Speck, *Journal of Applied Physics* **3**, 035702 (2019),]

A. Introduction

The band gaps of the InAlN alloy system span almost a full order of magnitude of energies from ~0.69 eV[1] for InN to ~6.2 eV[2] for AlN which also crossed the entire visible range. This makes the alloy system potentially useful for band gap engineering in the IR, visible, and UV ranges. The bandgap of InAlN, like many alloys, is known to have a nonlinear dependence on composition, this is called band gap bowing. Quantifying the band gap bowing is necessary to predict the band gap of an InAlN film of arbitrary composition.

There are examples of the measured dependence of the InAlN band gap on composition in the literature, however much of the older work was complicated by the lack of consensus on the band gap of InN at the time. Previously the InN bandgap was believed to be ~1.97 eV but the current consensus is that the band gap is ~0.69 eV.[1] This discrepancy resulted in some authors reach erroneous conclusions. Additionally much of the existing work focuses on compositions near $In_{0.18}Al_{0.72}N$ which is lattice matched with GaN and has been used as a barrier layer in HEMT structures.[3, 4] For the use of InAlN alloys in applications where a smaller band gap is necessary such as visible and IR devices, as well as for reporting values consistent with current understanding of the InN band gap, additional measurements are needed for the dependence of the InAlN band gap on composition. Since the InAlN band gap spans nearly an order of magnitude, fully characterizing the band gap of this system is of interest to the broader understanding of other extreme alloys such as BGaN[5-7] and BAlN.[8]

High quality InAlN films can be grown by a variety of methods including molecular beam epitaxy (MBE) and metalorganic chemical vapor deposition (MOCVD) which make it a good candidate for heterostructures with other III-nitride alloys[9-13] growth of InAlN films via MBE is complicated by the different incorporation efficiencies of the In and Al atoms.

Al incorporates into an InAlN film much more readily than In does. During most of the growth of an InAlN film this can be accounted for by having an In/Al flux ratio that is higher than the target In/Al ratio for the final film. However, it has been found that the InAlN growth must be initiated with a complete In adlayer (nominally ~two monolayer chemisorbed In wetting layer). If the In layer is not fully developed at the onset of InAlN growth, then a columnar InAlN likely results (referred to as a honeycomb microstructure).[10] The honeycomb structure is a result of Al rich initial nucleation events forming an Al rich platelet which are then surrounded by an In rich region. When the nucleation occurs in this way the microstructure and the lateral inhomogeneity propagates vertically in the growth direction.[11]

This paper will show results from independent measurements of composition and band gap from a series of high In content InAlN films grown on freestanding GaN. The growth techniques used were recently determined to result in homogeneous InAlN films without the common honeycomb microstructure. The band gap was derived from fitting the absorbance data using a Tauc plot method.

B. Experimental

Using previously developed InAlN growth methods for high In content without a honeycomb microstructure[10-12] a series of $In_xAl_{1-x}N$ thin films, 200 ± 20 nm thick, were grown on freestanding GaN substrates with x= 0.61, 0.69, 0.73, 0.81, 0.87, and 0.93. The freestanding GaN substrates were prepared with 500 nm of titanium deposited onto the back (N-face non-polished) side via e-beam metal deposition. The Ti layer acts as an IR absorber which enables better heating of the substrate in vacuum via radiative heating and also serves as a signal layer for IR pyrometery which allows in situ temperature measurements during growth. The pyrometer was calibrated to the film surface using the melting point of aluminum on a test substrate.

The samples were grown using a Varian Mod Gen II MBE using conventional In and Al effusion cells and a Veeco Unibulb RF-plasma unit. The plasma unit converts high purity N_2 gas into atomic nitrogen (N) which is readily incorporated into the film.[14] All films were grown in an N-rich regime with an N flux greater than the combined group III flux and at low temperatures < 450° C. Despite the excess N under these conditions, there is a metal adlayer on the surface due to the finite solubility of In in the InAlN film. The N flux was held at 8.0×10^{14} atoms/cm^{2}s. The In and Al fluxes were measured in situ using an ion gauge pressure sensor which reads in units of beam equivalent pressure. The In flux was held at a beam equivalent pressure of 1×10^{-7} Torr, the Al flux was varied from 2.5×10^{-9} Torr to 1.5×10^{-8} Torr. In all cases the large excess In flux allows for the rapid formation of an In adlayer which results in homogeneous growth.

High resolution X-ray diffraction (HRXRD) was used to determine the InAlN layer thickness and crystal quality using a Philips Panalytical MRD PRO diffractometer with a

four bounce Ge (220) monochromater using Cu-$K\alpha_1$ incident radiation (λ = 1.5405 Å). For on axis ω-2θ scans the signal was collected using a sealed proportional counter detector and a two bounce Ge (220) analyzer crystal. Most InAlN films showed clear thickness fringes in the ω-2θ, 0002 scans and thus the film thickness could be directly determined. Reciprocal space maps (RSMs) around the off axis $\bar{1}015$ peaks were measured using a PIXcel^{3D} detector in 2D mode. The a and c lattice parameters of the films were determined by fitting 2D Gaussians to the RSM peaks, determining the peak separation between the film and substrate peaks, then calculating the films parameters relative to the known substrate parameters.

After InAlN film growth, the Ti backing layers on the GaN substrates were removed via mechanical polishing. The dependence of the film absorbance on photon energy was measured using a Shimadzu UV-3600 UV-VIS-NIR Spectrometer. The band gaps were derived from the absorbance data via a Tauc plot method which has been previously shown in the literature[15-19] and is described in detail later in this paper.

C. Results

HRXRD scans of the 0002 peaks show that the $In_xAl_{1-x}N$ films have a wide variation in compositions. In Figure 2.1a the GaN substrate peak position is plotted to be constant and the comparative angular position of the lower intensity film peak can be seen varying as a function of composition. By measuring the angular separation between the substrate and the film peak we determined the c lattice parameter of the films. It can be seen in Figure 2.1a that the films with compositions up to x = 0.7 show thickness fringes indicative of high crystal quality films. Samples with In content above x = 0.7 do not show thickness fringes indicating lower crystal quality in this extremely lattice mismatched regime.

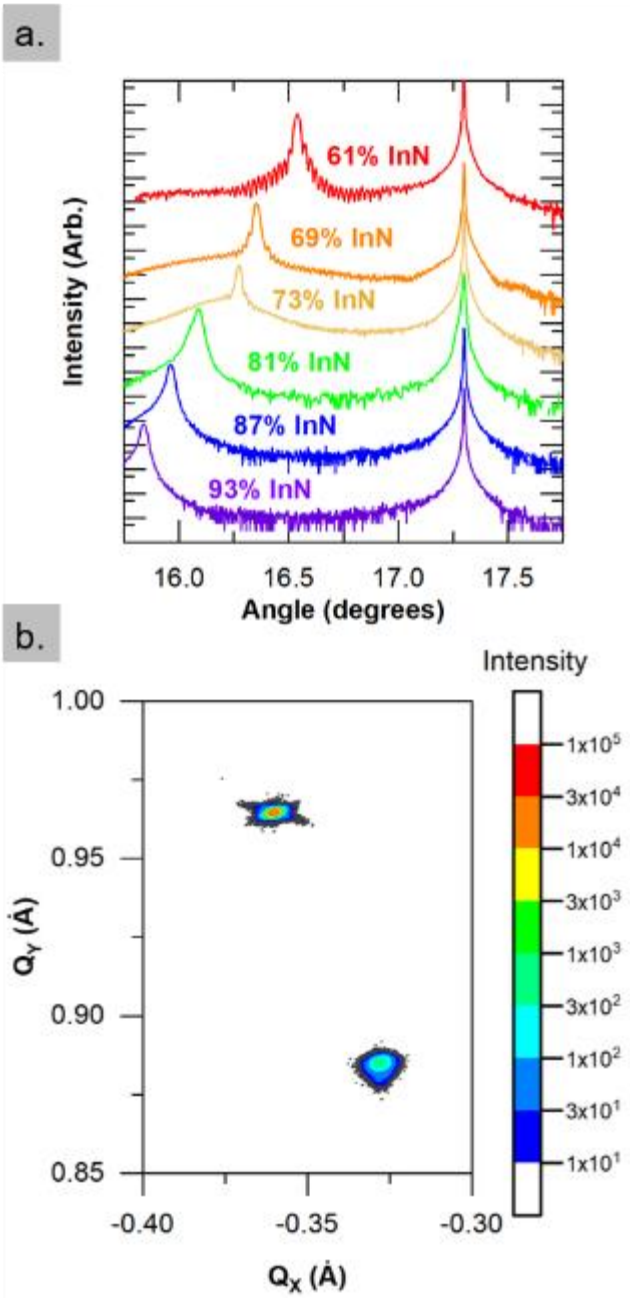

Figure 2.1 HRXRD Data (a) 0002 ω-2θ scans, peak separation is indicative of c spacing and therefore composition (b) Representative RSM of the $In_{0.93}Al_{0.07}N$ sample $\bar{1}015$ peaks from which the a and c parameters of the film were determined.

RSMs of the off axis $\bar{1}015$ peaks were used to determine the relaxation state of the films, the a lattice parameter, and an independent verification of the c lattice parameter. Figure 2.1b shows a RSM for the x = 0.93 film which is representative for all samples. The substrate and film peak positions were determined using a 2D Gaussian fit performed using commercial fitting software (OriginPro 2018). From the peak separations in reciprocal space, the lattice constants of the film can be determined relative to the known substrate lattice constants. The c parameters obtained using the two methods agree within expected instrument and fitting error. Using the a and c parameters and assuming the films were fully relaxed, we calculated film composition using Vegard's Law and literature values for the lattice constants of InN and AlN.[20] It was found that the compositions determined from both the a and c parameters were in agreement and therefore the assumption of a fully relaxed film was justified. The $In_xAl_{1-x}N$ compositions were x = 0.61, 0.69, 0.73, 0.81, 0.87, and 0.93. The lattice constants are reported in Table 2.1.

The band gap energies of the films were calculated from the absorbance data using a Tauc plot method.[21] In this method the product of the absorption coefficient squared and photon energy ($\alpha^2 h\nu$) is plotted vs photon energy ($h\nu$). The linear region of the plot is extrapolated to intercept with the energy axis which yields the band gap of the material. Figure 2.2a shows Tauc plot curves and the linear fits for each film.

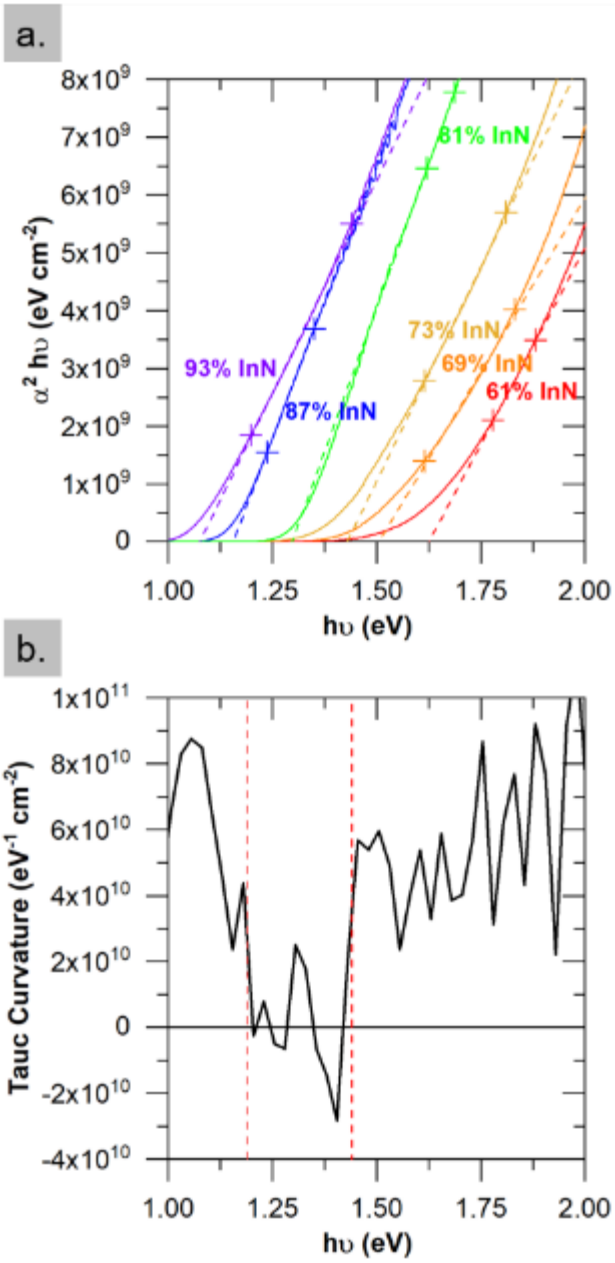

Figure 2.2. Tauc Plot (a) $\alpha^2 h\nu$ vs $h\nu$ data for our samples. Solid lines are experimental data, dashed lines are linear fits. (b) Representative curvature data for the $In_{0.93}Al_{0.07}N$ sample. The low-curvature fitting region is marked by crosses in a and by vertical dashed lines in b.

The Tauc plot analysis assumes a parabolic dispersion relation ($E_C = \frac{\hbar^2 k^2}{2m_e^*}$ and $E_V = \frac{\hbar^2 k^2}{2m_h^*}$) in both the conduction band and valence band and a direct transition for absorption in the material. Under those assumptions the absorption coefficient, α, is expected to increase with photon energy in a near band gap region such that,[21]

$$\alpha^2 h\nu = \beta(h\nu - E_g) \tag{2.1}$$

$$\beta \approx \frac{q^2\left(2\frac{m_h^* m_e^*}{m_h^* + m_e^*}\right)^{3/2}}{nch^2 m_e^*} \tag{2.2}$$

Here h is Planck's constant, ν is the photon frequency (making hν photon energy), α is the absorption coefficient, q is the fundamental charge, and c is the speed of light. The remaining values are material properties E_g is the band gap, n is the index of refraction, m_h^* and m_e^* are the hole and electron effective masses respectively. This analysis assumes that over some near, above band gap region we can assume β is a constant and that by fitting the data from that region to Equation 2.1 we can calculate the band gap.

For InN it is known that the bands become non-parabolic for photon energies less than 1 eV above band gap and therefore, particularly for In rich alloys, the scale of the fitting can have a large effect on the resultant band gap.[22] Such deviations from a parabolic band shape would result in β changing with photon energy since β is dependent upon reduced effective mass and therefore band curvature.

To ensure that we only fit the linear region of the data where our assumptions are valid we defined the linear region mathematically rather than by eye. To define the linear region first we calculated the curvature of each Tauc plot by interpolating the data points into a smooth function, taking the derivative with respect to energy, smoothing the resulting function by averaging over 0.1 eV, taking another derivative, and smoothing again over 0.1 eV. A representative plot of curvature data (specifically for the $In_{0.93}Al_{0.07}N$ sample) can be seen in Figure 2.2b. Ideally the linear region would have zero curvature however our real data has non-negligible noise around zero curvature. We selected a threshold value of 3 x 10^{10} eV^{-1} cm^{-2} which we determined to be just above the noise level for all samples and defined the liner region as the region with curvature values below that threshold. We then performed a linear fit of the $\alpha^2 h\nu$ vs $h\nu$ data in that region and calculated E_g using Equation 2.1. Interpolations and derivatives were performed using commercial software (Wolfram Mathematica 10). The values of E_g and β are reported in Table 2.1.

Table 2.1 Experimental Results for $In_xAl_{1-x}N$ films. In compositions (x), and lattice constants (c, a) derived from HRXIRD. Band gaps (E_g) and β values derived from Tauc plots.

x	c (Å)	a (Å)	E_g (eV)	β (cm^{-2})
0.61	5.42	3.36	1.63	1.20 x 10^{10}
0.69	5.53	3.43	1.50	1.36 x 10^{10}
0.73	5.54	3.45	1.43	1.48 x 10^{10}
0.81	5.57	3.48	1.30	1.90 x 10^{10}
0.87	5.61	3.50	1.16	1.99 x 10^{10}
0.93	5.65	3.51	1.08	1.47 x 10^{10}

All values have and error on order of ± 1%

We calculated a bowing parameter, b (see the discussion below), of 4.0 ± 0.2 eV using our experimental data and literature values for the band gaps of AlN and InN of 6.2 eV^2 and

0.69 eV[1] respectively. Figure 2.3 shows a scatter plot of our experimental data, a one parameter fit using the bowing parameter of 4.0 ± 0.2 eV, and literature values for epitaxial $In_xAl_{1-x}N$ films for comparison. [13, 17-19, 23-29]

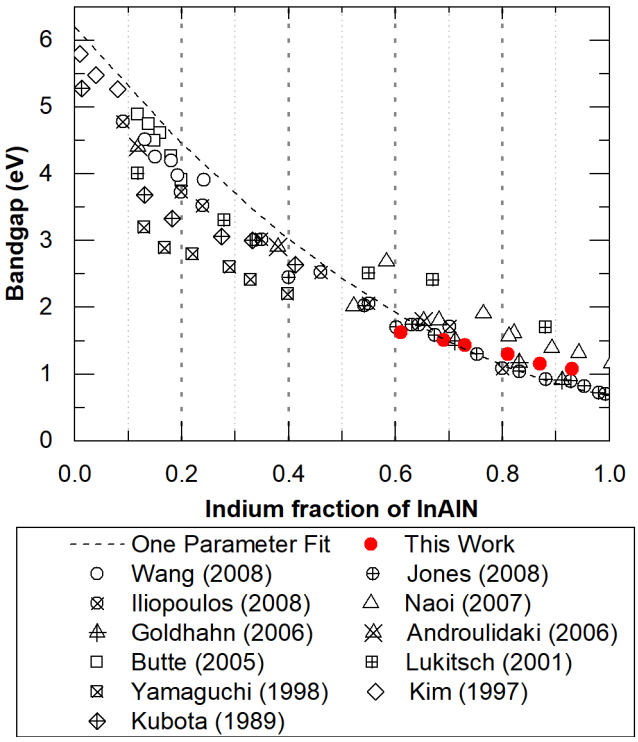

Figure 2.3. Bandgap vs Indium Fraction This work (closed red circles) which has error equivalent to the circle size, an experimental one parameter fit using a band bowing parameter of 4.0 eV (dashed line), and experimental results from the literature.

D. Discussion

The lattice parameters of III-nitride alloys have been shown to closely follow a linear variation with composition known as Vegard's Law.[30] There has been some evidence in the literature of deviations from Vegard's Law[27, 31] however such deviations are small and difficult to definitively distinguish from experimental error. For this paper we will assume that Vegard's Law holds for the unstrained lattice parameters of the InAlN system.

The band gap of most materials does not follow Vegard's Law, this deviation from a linear relationship is generally described with the following expression:

$$E_{gap}^{A-B}(x) = (x)E_{gap}^{A} + (1-x)E_{gap}^{B} - (x)(1-x)\mathrm{b} \qquad (2.3)$$

Where E_{gap}^{A-B} is the band gap at some composition x between two materials with band gaps $E_{gap}^{A}$and E_{gap}^{B}. In this work x is the group III composition of $In_xAl_{1-x}N$ and the two materials A and B are InN and AlN and b is the bowing parameter. To a first approximation b can be taken as invariant with composition. In this work we calculated a composition-independent band bowing parameter of b = 4.0 ± 0.2 eV which is in general agreement with the literature values as can be seen in Figure 2.3.

There is significant evidence in the literature that a composition-dependent bowing parameter more accurately fits the experimental and theoretical data for InAlN band gaps.[21, 32, 33] However there is not a broad consensus as to what functional form such a composition-dependent bowing parameter should take. A two or more parameter fit would fit the data better but without a known functional form with strong theoretical justification there is a risk

of overfitting the data. Band gap values for the pure compounds are also a potential source for error in the bowing parameter fit. Historically there was uncertainty as to the proper band gap for InN and currently there is similar uncertainty in the band gap of AlN. In this work the bowing parameter was calculated using E_{gap}^{AlN}= 6.2 eV.[2] If a different literature value for E_{gap}^{AlN} was used the resultant bowing parameter would be different. For example for E_{gap}^{AlN}= 6.1 eV[34, 35] or E_{gap}^{AlN}= 6.28 eV[36] the resultant bowing parameter fit to the data would be 3.8 eV or 4.1 eV respectively. It is clear that a composition-independent bowing parameter is a poor empirical fit to the experimental data. Therefore while the composition-independent bowing parameter is presented due to its ease of use for comparison to previous results the authors believe the data presented in Table 2.1 is the more accurate description of the results.

It is notable that the measured band gaps for our highest In content films trend higher than some literature values and if directly interpolated would point to an InN band gap of 0.8-1.0 eV which is inconsistent with the current understanding of the InN ~0.69 eV band gap for InN.[1] It is possible that compositional fluctuations could cause a Stokes shift similar to the results of Naoi et al.[28] or Androulidaki et al.[29] However the more likely cause of this discrepancy is a Moss-Burstein shit[37] caused by excess electrons in the high InAlN layers with the highest In content. The junction between GaN and InN is a type I straddling band gap heterojunction with a large conduction band offset of 2.3 eV.[38] With such an extreme offset the formation of a heterojunction leads to Fermi level pinning at the interface above the InN conduction band.[39, 40] It is likely that at some high In composition an InAlN/GaN junction the band offset would be large enough to similarly have E_f pinned above E_c at the InAlN at the interface. In such a situation the states at the bottom of the conduction band

near the interface would be filled and photons of energy E_g would not be absorbed. This would result in an over-estimate of the band gap from our absorption based measurement known as a Moss-Burstein shift.[37] Since our films are ~100 nm thick grown on GaN substrates it is reasonable to expect that their absorption behavior may be dominated by the heterojunction interface.

In this experiment the InAlN films were grown on freestanding GaN substrates in contrast to most of the literature which grows on sapphire substrates or on a GaN or AlN template. This difference in substrate appears to have had no impact on the band gaps which is consistent with InAlN films fully relaxed.

Using HRXRD on wurtzite structure III-nitride crystals is a well-established method for determining film properties. A common HRXRD measurement is the on-axis 0002 ω-2θ scan from which one can directly measure the c parameter of a film relative to the substrate and, if fringes are present, the thickness.

In order to determine the a parameter of a film without first knowing the strain state and compositions the HRXRD technique is a pair of off axis ω measurements.[41] In this measurement scheme an open detector is used and an omega scan is performed around a pair of off axis substrate peaks rotated 180° around the film normal such as $10\bar{1}5$ and $\bar{1}015$. Using the separation in omega between the film and substrate peaks in these two geometries the a and c parameter can be determined as was described by Krost et al.[41] In the course of this experiment we initially tried to use the paired off axis technique to independently measure the a and c parameters of the InAlN films but found that it did not work across all compositions. We determined that the experiment was limited by the angular range 2θ of our open detector 1.8°. It was determined that for high In InAlN films the a/c parameter is

sufficiently different that for many compositions some or all of the off axis peak intensity falls outside of our scanning range. Due to this limitation of the system we used RSMs of the off axis peaks to measure the a parameter which in our case has lower resolution than the paired off axis technique due to instrument limitations.

In this experiment we used the Tauc relation to determine the band gaps of our films. This required us to perform linear fits to sets of data which are imperfectly linear. Rather than fit by eye we decided to interpolate our data into a smooth function and derivate that function twice in order to find the curvature of the data then select a region with curvature near zero in the noise level, in this case lower than $3 \times 10^{10}\ eV^{-1}cm^{-2}$.

E. Conclusion

In conclusion a series of $In_xAl_{1-x}N$ thin films were grown via Plasma Assisted MBE on freestanding GaN substrates with compositions ranging from x = 0.61 to x = 0.93. Compositions were determined via HRXRD and assuming Vegard's Law for lattice constants. Band gaps were measured independently via absorption measurements with the absorption coefficients fitted in a Tauc plot model. The resulting band gap and composition data is presented above in Table 2.1. To compare the results from this experiment to the literature the data was fitted to a simple one parameter band bowing model and a composition-independent band bowing parameter of 4.0 ± 0.2 eV was calculated. The results are in general agreement with the literature.

Acknowledgements

Funded by a grant from the NSF Award No. DMR 1434854. The MRL Central Facilities are supported by the MRSEC Program of the NSF under Award No. DMR 1121053; a member of the NSF-funded Materials Research Facilities Network (www.mrfn.org). Additional support was provided by the CREST program at UCSB.

Chapter 2 References

[1] J. Wu, W. Walukiewicz, W. Shan, K.M. Yu, J.W. Ager III, S.X. Li, E.E. Haller, H. Lu, and W.J. Schaff, J. Appl. Phys. 94, 4457 (2003).

[2] L. Chen, B.J. Skromme, R.F. Dalmau, R. Schlesser, Z. Sitar, C. Chen, W. Sun, J. Yang, M.A. Khan, M.L. Nakarmi, J.Y. Lin, and H.X. Jiang, Appl. Phys. Lett. 85, 4334 (2004).

[3] D.S. Lee, X. Gao, S.P. Guo, D. Kopp, P. Fay, T. Palacios, IEEE Electr. Device L. 32, 1525 (2011).

[4] Y. Yue, Z. Hu, J. Guo, B. Sensale-Rodriguez, G. Li, R. Wang, F. Faria, T. Fang, B. Song, X. Gao, S. Guo, T. Kosel, G. Snider, P. Fay, D. Jena, H. Xing, IEEE Electr. Device L. 33, 988 (2012).

[5] R.C. Cramer, B. Bonef, J. English, C.E. Dreyer, C.G. Van de Walle, J. S. Speck, J. Vac. Sci. Technol. A 35, 041509 (2017)

[6] B. Bonef, R. Cramer, J.S. Speck, J. Appl. Phys. 121, 225701 (2017)

[7] C.E. Dreyer, J.L. Lyons, A. Janotti, C.G. Van de Walle, Appl. Phys. Lett. 7, 031001 (2014)

[8] J.X. Shen, D. Wickramarantne, C.G. Van de Walle, Phys. Rev. Materials 1, 065001 (2017)

[9] D.F. Brown, S. Keller, T.E. Mates, J.S. Speck, S.P. DenBaars, U.K. Mishra, J. Appl. Phys. 107, 033509 (2010)

[10] E.C.H. Kyle, S.W. Kaun, F. Wu, B. Bonef, J.S. Speck, J. Cryst. Growth 454, 164 (2016).

[11] E. Ahmadi, R. Shivaraman, F. Wu, S. Wienecke, S. W. Kaun, S. Keller, J. S. Speck, U. K. Mishra, Appl. Phys. Lett. 104, 072107 (2014).

[12] M.J. Lukitsch, Y.V. Danylyuk, V.M. Naik, C. Huang, G.W. Auner, L. Rimai, R. Naik, Appl. Phys. Lett. 79, 632 (2001).

[13] S. Choi, F. Wu, R. Shivaraman, E.C. Young, J.S. Speck, Appl. Phys. Lett. 100, 232102 (2012)

[14] S. Agarwal, B. Hoex, M.C.M. Van de Sanden, D. Maroudas, E.S. Aydil, Appl. Phys. Lett. 83, 4918 (2003)

[15] Q. Guo, T. Tanaka, M. Nishio, H. Ogawa, Jpn. J. Appl. Phys. 42, L 141 (2003).

[16] R.E. Jones, R. Roesler, K.M. Yu, J. W. Ager III, E.E. Haller, W. Walukewicz, X. Chen, W.J. Schaff, J. Appl. Phys. 104, 123501 (2008).

[17] K.S. Kim, A. Saxler, P. Kung, M. Raxeghi, Appl. Phys. Lett. 72, 800 (1997).

[18] S. Yamaguchi, M. Kariya, S. Nitta, H. Kato, T. Takeuchi, C. Wetzel, H. Amano, I. Akasaki, J. Crystl. Grow. 195, 309 (1998).

[19] T. Peng, J. Piprek, G. Qiu, J. O. Olowolafe, K. M. Unruh, C. P. Swann, and E. F. Schubert, Appl. Phys. Lett. 71, 2439 (1997).

[20] I. Vurgaftman, and J.R. Meyer, J. Appl. Phys. 94, 3675 (2003).

[21] J.I. Pankove, Optical Processes In Semiconductors, New York: Dover, (1975), Print

[22] P. Carrier, S.H. Wei, AIP Conf. Proc. 772 287 (2005)

[23] K. Wang, R. W. Martin, D. Amabile, P. R. Edwards, S. Hernandez, E. Nogales, K. P. O'Donnell, K. Lorenz, E.Alves, V. Matias, A. Vantomme, D. Wolverson, and I. M. Watson, J. Appl. Phys. 103, 073510 (2008).

[24] E. Iliopoulos, A. Adikimenakis, C. Giesen, M. Heuken, and A. Georgakilas Appl. Phys. Lett. 92, 191907 (2008);

[25] R. Goldhahn, P. Schley, A. T. Winzer, G. Gobsch, V. Cimalla, O. Ambacher, M. Rakel, C. Cobet, N. Esser, H. Lu, and W. J. Schaff, phys. stat. sol. (a) 203, 42 (2006).

[26] R. Butte, J.F. Carlin, E. Feltin, M. Gonschorek, S. Nicolay, G. Christmann, D. Simeonov, A. Castiglia, J. Dorsaz, H.J. Buehlmann, S. Christopoulos, G. Baldassarri, Hoger van Hogersthal, A.J.D. Grundy, M. Mosca, C. Pinquier, M.A. Py, F. Demangeot, J. Frandon, P.G. Lagoudakis, J.J. Baumberg, N. Grandjean, J. Phys. D Appl. Phys. 40, 6328 (2007).

[27] K. Kubota, Y. Kobayashi, and K. Fujimoto, J. Appl. Phys. 66, 2984 (1989).

[28] H. Naoi, K. Fujiwara, S. Takado, M. Kurouchi, D. Muto, T. Araki, H. Na, and Y. Nanishi, J. Electron. Mater. 36 1313 (2007)

[29] M. Androulidaki, N. T. Pelekanos, K. Tsagaraki, E. Dimakis, E. Iliopoulos, A. Adikimenakis, E. Bellet-Amalric, D. Jalabert, and A. Georgakilas, phys. stat. sol. (c) 3 1866 (2006)

[30] L. Vegard, Zeitschriftfür, Physik 5, 17 (1921).

[31] K. Lorenz, N. Franco, E. Alves, I.M. Watson, R.W. Martin, K.P. O'Donnel, Phys. Rev. Lett. 97, 08550 (2006).

[32] R. R. Pelá, C. Caetano, M. Marques, L. G. Ferreira, J. Furthmüller, and L. K. Teles, Appl. Phys. Lett. 98, 151907 (2011)

[33] S. Schulz, M. A. Caro1, L. Tan, P. J. Parbrook, R.W. Martin, and E.P. O'Reilly, Appl. Phys. Express 6 121001 (2013)

[34] M. Feneberg, R.A.R. Leute, B. Neuschl, K. Thonke, and M. Bickermann, Phys. Rev. B 82, 075208 (2010)

[35] V.Z Zubialevich, D.V. Dinh, S.N. Alam, S. Schulz, E.P. O'Reilly, and P.J. Parbrook, Semicond. Sci. Technol. 31 025006 (2016)

[36] L. Roskovcova, J. Pastrnak, Czech. J. Phys. B 30 586 (1980)

[37] K.S.A. Butcher, H. Hirshy, R.M. Perks, M. Winterbrert-Foquet, P. P.T. Chen, physica status solidi (a) 203, 66, (2006)

[38] C. G. Van de Walle and J. Neugebauer, Nature (London) **423**, 626 (2003)

[39] K.A. Wang, C. Lian, N. Su, D. Jena, and J. Timler, App. Phys. Lett **91**, 232117 (2017)

[40] S. Krishna TC, and G. Gupta, RCS Adv., **4**, 27308 (2014)

[41] A. Krost, G. Bauer, J. Woitok, Optical Characterization of Epitaxial Semiconductor Layers, Chapter 6, Springer: Berlin, (1996)

Chapter 3: Growth of coherent BGaN films using BBr_3 gas as a boron source in plasma assisted molecular beam epitaxy

Incorporating boron into gallium nitride to make $B_xGa_{1-x}N$ solid solutions would create an avenue for extreme alloys due to the large band gap and small lattice parameters wurtzite phase BN is predicted to have compared to GaN. In this paper we report the growth of high crystal quality, random alloy $B_xGa_{1-x}N$ thin films with x up to 3.04% grown on (0001) Ga-face GaN on sapphire substrates using plasma assisted molecular beam epitaxy and BBr_3 gas as a B source. High resolution X-ray diffraction was used to measure both the c plane spacing and the strain state of the films. It was determined that the films were fully coherent to the GaN substrate. Elastic stress-strain relations and Vegard's law were used to calculate the composition. Atom probe tomography was used to confirm that the $B_xGa_{1-x}N$ films were random alloys. In addition to demonstrating a growth technique for high crystal quality $B_xGa_{1-x}N$ thin films this paper demonstrated the use of BBr_3 as a novel B source in plasma assisted molecular beam epitaxy. Reproduced with permission from the Journal of Vacuum Science & Technology A [Growth of coherent BGaN films using BBr3 gas as a boron source in plasma assisted molecular beam epitaxy, Richard C. Cramer, Bastien Bonef, John English, Cyrus E. Dreyer, Chris G. Van de Walle, James S. Speck, *Journal of Vacuum Science and Technology A* **35**, 041509 (2017)]

A. Introduction

The III-nitride family of materials has demonstrated considerable uses in light emitting diodes,[1,2] laser diodes,[3,4] and high frequency power electronics.[5,6] Conventionally, this materials family consists of AlN, GaN, InN, and solid solution alloys of the three compounds. Incorporating the group III element boron into this family expands the paramater space of the III-nitride materials family and may allow for the creation of additional useful crystal alloys. Predictions of the properties of B containing III-nitride alloys are complicated by the fact that the stable phase of BN is hexagonal (layered structure) instead of the wurtzite structure of the conventional group III nitrides and consequently the physical and structural properties are not well documented. Density functional theory calculations predict that compared to the other III-nitrides, wurtzite BN would have a wide band gap, 10.13 eV direct gap, 6.46 eV indirect gap, and small lattice constants, a = 2.52 Å, c = 4.17 Å[7.] Vegard's law would therefore predict that successful incorporation of B into III-nitride alloys could have large effects on the band gap and lattice constant even at low B concentrations. If the above predictions prove true, BGaN could be useful as a barrier material for deep UV optoelectronics due to its high band gap. It may also be useful as a back barrier for high electron mobility transistors[8]. Additionally, previous experimental literature has shown BGaN to be potentially useful in forming lattice constant gradients between small a parameter substrates, such as 6H-SiC, and larger a parameter films such as GaN[9].

BGaN has been grown via metalorganic chemical vapor deposition (MOCVD)[10-14] and molecular beam epitaxy (MBE)[15] though the crystal quality in these experiments is poor compared to conventional III-nitrides. The extreme lattice mismatch between the wurtzite

phase of BN and the other III-nitrides could be responsible for this low quality. Addionally, growing high B concentration BGaN can lead to phase seperation and poor crystal quality. Previous reports calculate B concentration using high resolution x-ray diffraction (HRXRD) and assuming that the BGaN films are completely relaxed.

The BGaN samples reported in this paper were grown using plasma assisted molecular beam epitaxy (PAMBE) which is a common research technique for III-nitrides growth and in particular GaN. In PAMBE, nitrogen is provided via a N_2 plasma and the group III elements (In, Ga, and Al) and common dopants (Si, Mg) come from solid source effusion cells. Because of the high melting point of B, an effusion cell is less practical to introduce this element. It has been demonstrated previously that carbon, another high melting point material, can be used as a compensating dopant in PAMBE growth of GaN by using a CBr_4 gas source[16]. This was the motivation for this project where we used BBr_3 gas as a source for B.

In this paper, we report the growth of high crystal quality, single phase, BGaN thin films using BBr_3 gas as a boron source in PAMBE. We have demonstrated that this method can grow $B_xGa_{1-x}N$ films up to x = 3.04% while maintaining high crystal quality. To calculate the composition of the films, we measured the c plane spacing of the films using HRXRD. We then measured the strain state using HRXRD and determined that the films were fully strained to the GaN film substrate and therefore we used standard elastic stress-strain relations and Vegard's law to calculate their composition. Additionally, we used atom probe tomography (APT) to confirm that the BGaN films are random alloys.

B. Experimental

Samples were grown on conductive MOCVD Ga-face GaN:Si templates on sapphire (STN) purchased from St. Gobain (Lumilog). 500 nm of titanium metal were deposited onto the back, unpolished sapphire, side of the substrate, using an electron-beam evaporation system. The titanium layer provided even thermal spreading across the substrate and, when heated, serves as emissive layer for infrared pyrometry which is used to measure the substrate temperature.

The growth method used for BGaN films in this experiment is a variation of the well-established III-nitride PAMBE method of modulated growth. Modulated growth of GaN is a technique which has been demonstrated to achieve high crystal quality and good surface morphology[17]. During PAMBE growth of GaN, if the Ga flux exceeds the active nitrogen flux then the excess Ga may form a Ga adlayer. It has been demonstrated that the presence of this adlayer between 1 and 2.4 monolayers (MLs) improves the surface of the GaN crystal compared to the growth with an adlayer less than 1 ML. Increasing the adlayer thickness above 2.4 MLs causes Ga droplet formation which results in large (> 10 μm) morphological features on the surface. During modulated growth, the time average monolayer coverage is kept below 2.4 ML and all regions on the surface are transient with a condition of adlayer coverage above 2.4 ML. During modulated growth the Ga adlayer is monitored in situ via reflection high energy electron diffraction (RHEED). To characterize the adlayer, the intensity of a specular reflection spot is monitored over time. When the adlayer is forming, a decrease in intensity is observed with a characteristic shoulder at 1 ML. Similarly when the adlayer is dispersing, the intensity returns to its previous value again with a characteristic shoulder at 1 ML.

For BGaN layers the modulated growth technique for GaN described above is modified with the introduction of BBr_3 gas (99.999% purity, STREM Chemicals) through a showerhead injector. BBr_3 flow was controlled via the temperature of the BBr_3 source which was held constant at 0 °C which corresponds to a beam equivalent pressure of 3.76 x 10^{-7} Torr as measured by an ion gauge in the substrate position. We do not currently have a method to accurately convert this beam equivalent pressure into a B flux. However, if we assume that Ga and BBr_3 have the same conversion factor between the ion gauge measurement and the GaN equivalent growth rate then this flux would be 6 nm/min. It is likely that BBr_3 being a polyatomic molecule, it would have an ion gauge sensitivity factor greater than that of Ga though neither factor has been calculated or measured experimentally. This would make 6 nm/min an overestimate[18]. We therefore assumed that the BBr_3 flux was of order 1 to 10 nm/min.

In this set of experiments, samples were grown using a Varian Gen II molecular beam epitaxy system. Nitrogen was provided by flowing N_2 gas (99.9995% purity) at 1.3 sccm through a Veeco RF Unibulb source and excited into a plasma via 250 watts of RF radiation, this corresponds to 6.3 nm/min GaN equivalent growth rate of active nitrogen flux for all samples. For all samples the substrate temperature was held at a 720 °C as measured by infrared pyrometry of the Ti layer. Ga was provided using a Veeco SUMO cell. Seven samples were grown. Each sample consisted of two layers, a 100 nm unintentionally doped (UID) GaN layer grown with a Ga flux equal to 8.7 nm/min followed by a BGaN layer which was grown for 30 min total growth time. The growths were performed in 10 minutes segments with 5 minute growth interrupts between to allow the Ga adlayer to desorb. The BBr_3 flux was held constant at 3.76 x 10^{-7} Torr for all BGaN layers. A series of samples

was grown using varying Ga fluxes. Samples A, B, C, D, E, F, and G were grown using Ga fluxes of 7.9, 6.4, 5.7, 5.4, 4.9, 4.5, and 4.0 nm/min respectively. With constant BBr_3 flux and decreasing Ga flux the B composition of the films increases for samples A through sample G. All BGaN layers were grown with a Ga flux less than that of the pure GaN to prevent the total group III flux from being too high.

The crystal quality of the samples was characterized using high resolution X-ray diffraction (XRD) on a Philips Panalytical MRD PRO diffractometer with a four bounce Ge (220) monochromater using Cu-Kα1 incident radiation ($\lambda = 1.5405$ Å). The signal was collected using a sealed proportional counter detector and a two bounce Ge (220) analyzer crystal. Reciprocal space maps of the $\bar{1}015$ reflection condition were collected using a PIXcel^{3D} detector. The sample surfaces were characterized with atomic force microscopy (AFM) via an Asylum MFP-3D tool used in tapping mode in air.

After the XRD and AFM characterization of the samples. Sample F was selected to have further characterization via atom probe tomography (APT). The sample had a 100 nm GaN cap grown on top of the BGaN layer under the same conditions as the GaN buffer. The GaN cap facilitates the preparation of APT samples. The tip was prepared with a gallium ions FEI Helios 600 dual beam FIB instrument following standard procedure. A final milling with an acceleration voltage of 2 kV was used to minimize damage from the preparation[19]. APT analysis was performed with a Cameca 3000X HR Local Electrode Atom Probe (LEAP) operated in laser-pulse mode (13 ps pulse, 532 nm green laser, 10 µm laser spot size) with a sample temperature of 45 K. The laser pulse energy was 1 nJ and a detection rate of 0.005 atoms per pulse was set during the analysis. APT 3D reconstruction

was carried out using commercial software IVASTM with the scanning electron microscopy image of the tip used as a reference[20].

C. Results

The image in Figure 3.1 (a) shows the RHEED pattern that was observed during a GaN buffer layer growth; an arc of RHEED spots that is characteristic of a 2D surface. The GaN buffer layer was grown in a method consistent with previous reports[17]. During the buffer growth, the RHEED dimmed and brightened as the adlayer was formed and desorbed. During the growth of the BGaN layer for sample A, the RHEED intensity dimmed indicating the presence of a surface adlayer though the overall intensity variation was smaller compared to the one observed in the GaN buffer layer growth. During the growth of the BGaN layers for sample B through G, the surface underwent a transition from a smooth flat surface, to a three dimensional surface. The images in Figure 3.1 (b), and (c) show the spotty RHEED pattern characteristic of a 3D surface for the conditions of the incident beam parallel to the $\langle 1\bar{1}00 \rangle$ and $\langle 2\bar{1}\bar{1}0 \rangle$ directions respectively. The RHEED patterns for both azimuths show that the BGaN sustains the same hexagonal structure as the underlying GaN. Weak chevrons were observed in the $\langle 1\bar{1}00 \rangle$ azimuth condition which indicates faceting of the $\{10\bar{1}3\}$ family of planes, this is consistent with the rough surface morphology that has been previously observed for N rich growth of GaN[21]. The three dimensional RHEED pattern did not change in intensity during growth which prohibited the measurement of a group III adlayer in the same way that it is done when growing smooth GaN. Despite the lack of evidence for an adlayer in the RHEED for sample B it was found that periodic growth interrupts were needed to maintain high crystal quality. Samples grown under the same conditions as sample B but without the periodic growth interrupts had fewer fringes and had droplets on the surface. Therefore all growths were performed with periodic growth interrupts as is normal for modulated growth.

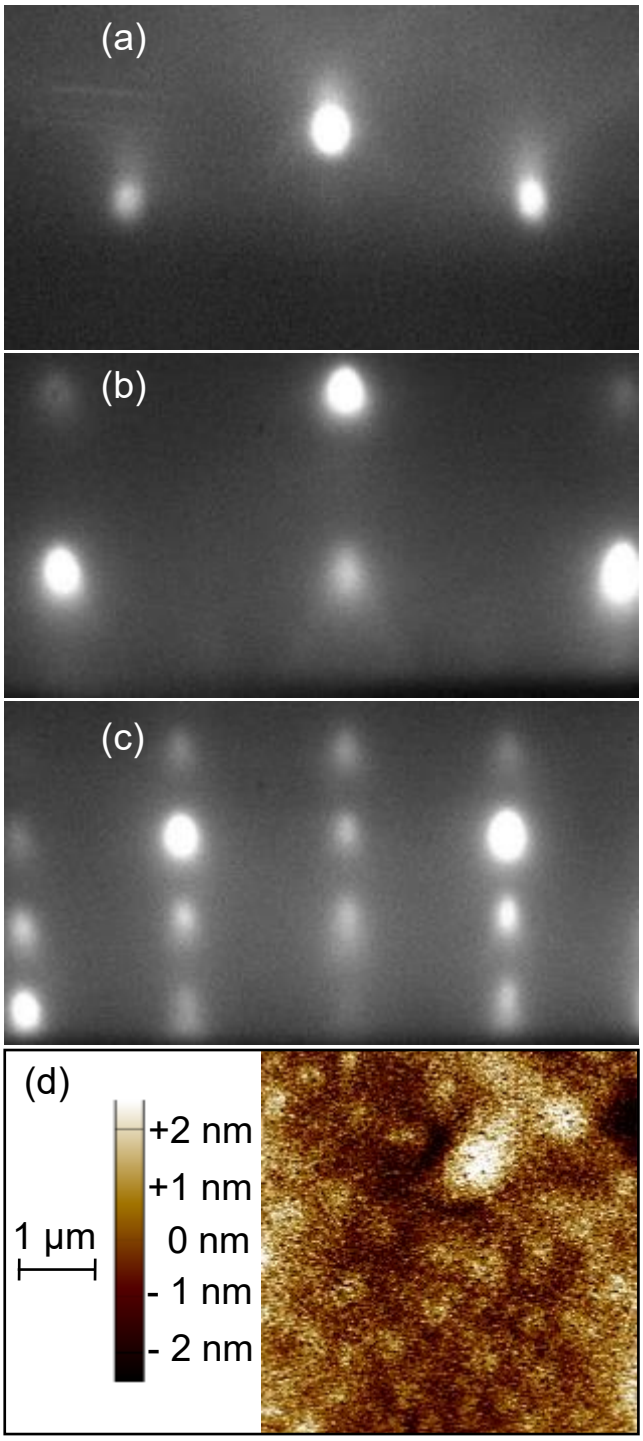

Figure 3.1 Surface characterization of BGaN
(a) RHEED pattern obtained from a 2D growth of GaN (b) 3D RHEED pattern obtained during growth of a BGaN film with incident beam parallel to ⟨$\mathbf{1\bar{1}00}$⟩, (c) the same film as b rotated 30° so the incident beam is parallel to ⟨$\mathbf{2\bar{1}\bar{1}0}$⟩. (d) AFM 5x5 μm scan of sample F, the surface is rough with no discernible step edges**.**

AFM was performed on all samples. Sample A was found to have large droplets on the surface consistent with what is observed during modulated growth with too high of a Ga flux. Since Sample A was grown using a Ga flux less than the flux used for GaN, which does not result in droplets, this indicates that B from the BBr_3 was contributing to a group III adlayer or to droplet formation in some way. Samples B through G were found to have a generally rough surface morphology with no discernable facets or step edges and a RMS roughness ~2 nm. A 5x5 μm AFM scan of sample F is shown in Figure 3.1, samples B through G are similar.

On axis 0002 ω-2θ XRD scans of the samples are shown in Figure 3.2. The figure shows the results of all seven samples plotted on a log scale with vertical offsets. By measuring the angular separation between the GaN substrate peak and the BGaN film peak in the 0002 scan, the c parameter of the films is directly determined using well established crystallographic relations, we will relate this to composition later in this section. Sample A does not have a secondary peak indicating that there was no incorporation of B into the crystal under those growth conditions. Samples B through F show a secondary peak which is a result of B incorporation in the BGaN layer and thickness fringes out to at least third order which is indicative of high crystal quality. Sample G has a secondary peak but does not have fringes which indicates B incorporation but lower crystal quality than samples B through F. The spacing of the secondary peak fringes was used to calculate BGaN layer thicknesses and growth rate when applicable, this is shown in Table 3.1. It can be seen that decreasing the Ga flux decreases the total group III flux and resulted in a lower growth rate and therefore a smaller overall thickness since all BGaN layers had a total growth time of 30 minutes.

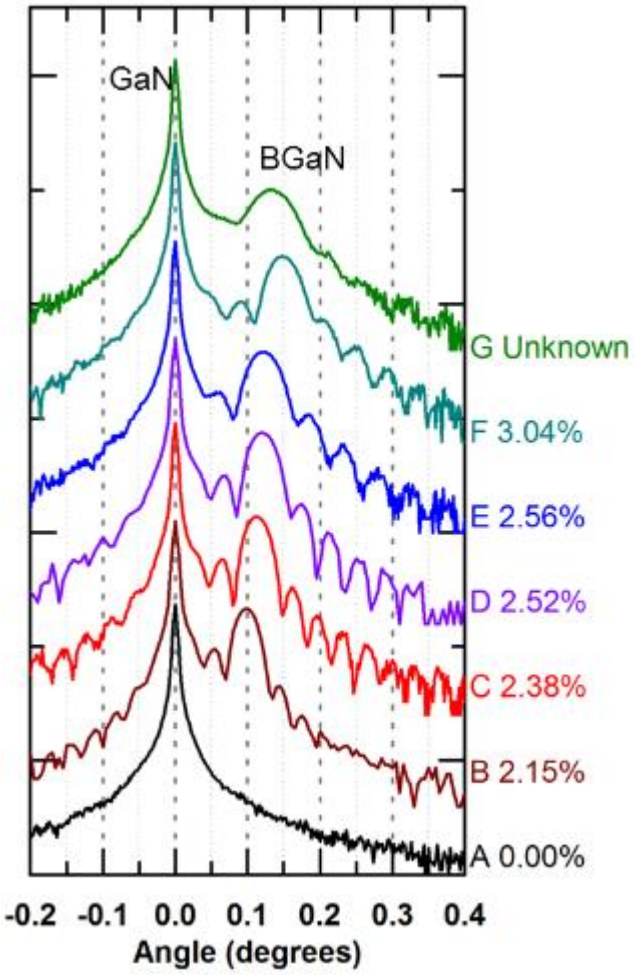

Figure 3.2 On-axis XRD 0002 ω-2θ scans of five BGaN samples with different boron composition.
Vertical scale is a log scale with offsets for clarity, vertical units are otherwise arbitrary. The angle is delta omega from the GaN substrate peak. The angular separation between the film and substrate peaks correlate with B concentration for samples with the same strain state (B through F). The presence of thickness fringes is indicative of high crystal quality films. Sample A shows no boron incorporation. Sample G shows low crystal quality.

Table 3.1. $B_xGa_{1-x}N$ film properties.

Sample	Ga Flux (nm/min)	x	Thickness (nm)	Growth Rate (nm/min)
A	7.9	0.00%	-	-
B	6.4	2.15%	145	4.8
C	5.7	2.38%	134	4.5
D	5.4	2.52%	121	4.0
E	4.9	2.56%	101	3.3
F	4.5	3.04%	101	3.3
G	4.0	-	-	-

N Flux = 6.3 nm/min for all samples

Figure 3.3 (a) shows a diagram of the accessible XRD points in the wurtzite GaN system in reciprocal space. We measured the 0002 ω-2θ scans to determine the c spacing of the film. To accurately calculate the composition we first determined the strain state by measuring a reciprocal space map (RSM) for each sample. Each RSM covers an area of 3° in omega and 2.5° degrees in theta around the $\bar{1}015$ GaN substrate peak. The RSMs obtained for samples B through G are displayed in Figure 3.3 (b). The large signal in the center is the GaN substrate peak and the smaller signal above is the BGaN film peak. The vertical spacing between the peaks is indicative of the B concentration and shows the same trend as the 0002 measurements. The lateral peak position for each film matches the lateral peak position of the GaN peak which shows that the films are fully coherent with the substrates and therefore fully strained. The RSM for sample A is not shown because it has no secondary peak and did not provide any new information. The RSM for sample G did not have a defined BGaN peak but rather a diffuse intensity both above and to the left of the GaN peak. This indicates some degree of relaxation or other multiple phases but overall was inconclusive. Combined with the low crystal quality of sample G, this leads us to conclude that sample G was not grown with promising growth conditions. The samples that

are fully strained are the same samples that show fringing in Figure 3.2, they all share the same strain state and can be directly compared with a larger angular separation between the GaN and BGaN peaks correlating directly with B composition. Sample G however has a smaller angular separation despite being grown in conditions that one would expect to lead to a higher B concentration. This discrepancy is due to relaxation and overall decrease in crystal quality of the film. The following analysis will focus on the high crystal quality, coherent samples B to F from which we can accurately calculate composition.

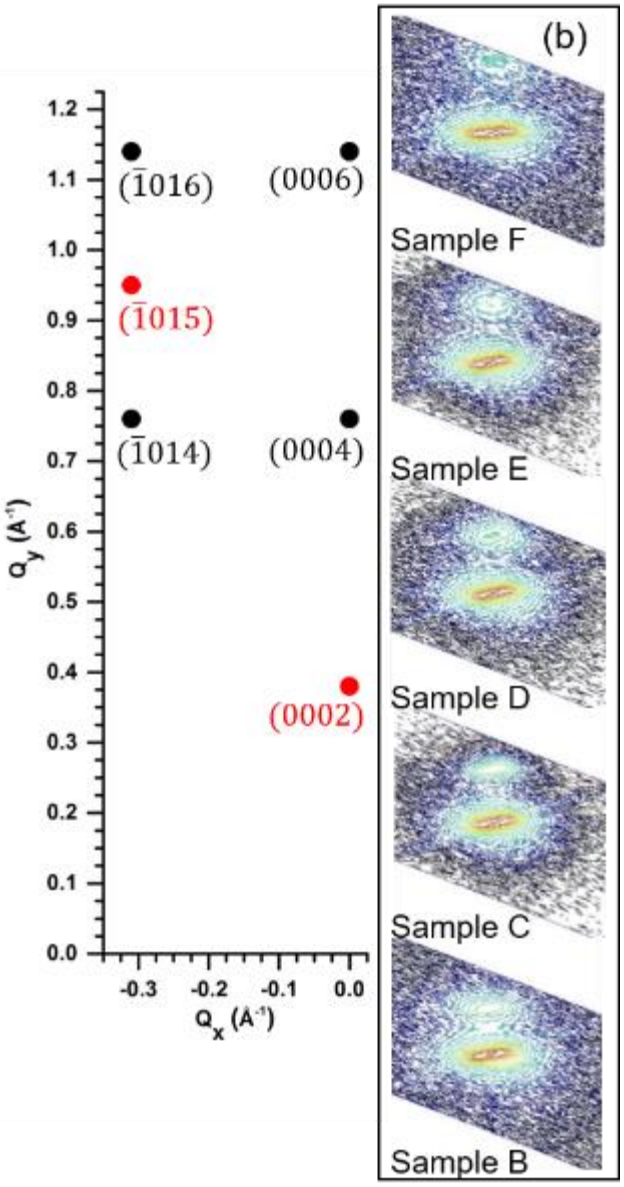

Figure 3.3 Reciprocal space maps.
(a) Diagram of the accessible XRD points in the wurtzite GaN system. The measured points 0002 and $\bar{1}015$ are shown in red. (b) RSM for the five high crystal quality samples. The low intensity BGaN film peak is directly vertical of the substrate peak indicating a fully coherent film for these samples

For samples B through F the composition x of the $B_xGa_{1-x}N$ films was calculated assuming Vegard's law[22]. The unstrained lattice parameters of wurtzite GaN, $a_{GaN,o}$ and $c_{GaN,o}$, were taken from experimental literature[23]. The unstrained lattice parameters for wurtzite BN, $a_{BN,o}$ and $c_{BN,o}$, were taken from a density functional results since wurtzite is not the stable phase of BN under normal conditions[7]. According to Vegard's law the relations between the unstrained lattice parameters of the $B_xGa_{1-x}N$ film of composition x, $a_{BGaN,o}$ and $c_{BGaN,o}$, the unstrained lattice parameters of BN, $a_{BN,o}$ and $c_{BN,o}$, and GaN, $a_{GaN,o}$ and $c_{GaN,o}$, are:

$$c_{BGaN,o} = c_{BN,o}(x) + (1-x)c_{GaN,o} \qquad (3.1)$$

$$a_{BGaN,o} = a_{BN,o}(x) + (1-x)a_{GaN,o} \qquad (3.2)$$

To relate the strained c lattice parameter that is extracted from the 0002 XRD measurement, $c_{measured}^{BGaN}$, to the unstrained lattice constant for $B_xGa_{1-x}N$ of composition x standard strain tensors are used. Since the films were mostly GaN, the elastic parameters of GaN, C_{13} and C_{33}, measured by Wright *et al.*[24] are used. With a fully coherent film, the tensor equation reduces to the following:

$$c_{measured}^{BGaN} = \left(c_{BGaN,o}\right) - c_{GaN}\left(\frac{2\,C_{13}}{C_{33}}\right)\left(\frac{a_{BGaN,o} - a_{GaN,o}}{a_{GaN,o}}\right) \qquad (3.3)$$

By simultaneously solving the above three equations the composition x of the $B_xGa_{1-x}N$ films can be obtained. The results of this calculation are shown in Table 3.1.

Figure 3.4 (a) shows a 2D distribution of boron extracted from the APT reconstruction of sample F. On this image, highly concentrated boron clusters (above 8 at%) can not be seen and the alloy distribution is consistent with a random distribution. The presence of these B rich and poor regions is not caused by any clustering driving force but only caused by intrinsic desorder during growth. The III site boron concentration obtained from the 3D volume in the BGaN layer is 3.0 atom % which is in very good agreement with the XRD measurements and analysis based on coherent films and Vegard's Law. Figure 3.4 (b) is the distribution of B composition for bins of a 15x40x70 nm^3 sampling volume extracted in the 3D reconstruction. The volume is subdivided in 2090 sampling volumes of 100 atoms in which the boron fraction is measured. The experimental distribution of boron is compared with the binomial distribution expected for a random alloy[25]. A χ^2 test is used to quantitatively compare the two distribution. A χ^2 value of 16.4 is obtained for 11 degrees of freedom wich correponds to a p value above 0.1. A p value above 0.1 confirms the hypothesis that BGaN is a random alloy. The same test was performed with sampling volumes composed of 50, 150 and 200 atoms and in different location in the BGaN layer which all resulted in the success of the χ^2 test. B in the BGaN layer is randomly distributed and clustering effects are not observed. Br which could originate from the BBr_3 source was not detected in the APT mass spectrum.

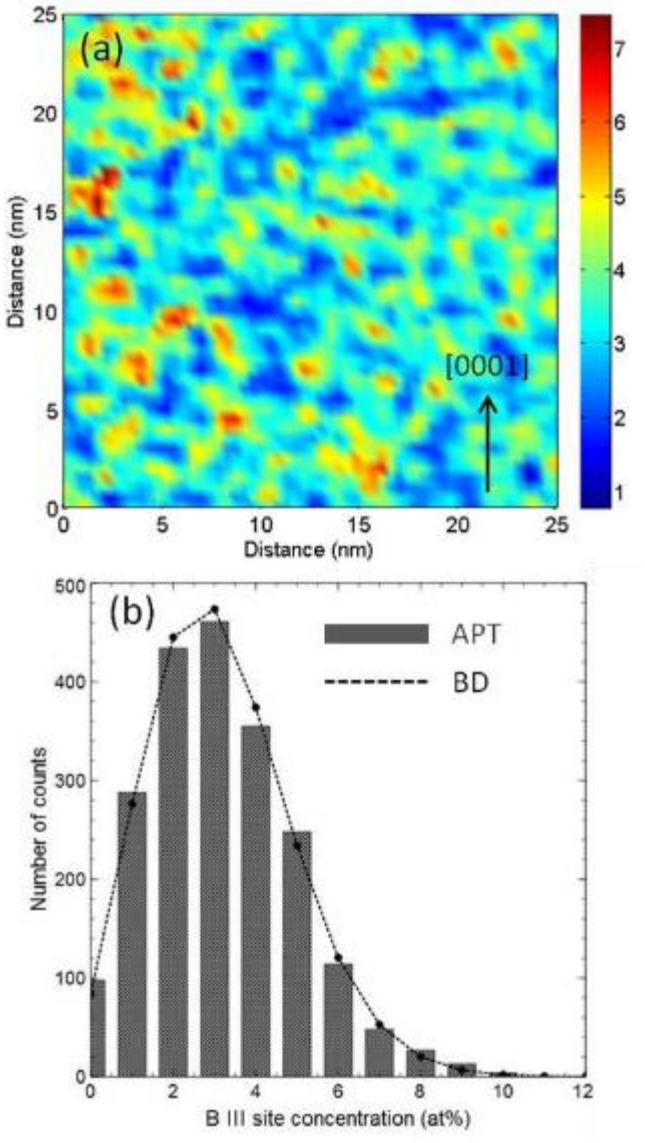

Figure 3.4 APT composition results of sample F.
(a) 2D distribution of boron extracted from the APT reconstructed volume (b) Statistical distribution analysis of boron in the BGaN layer. The dashed line shows the binomial distribution that is expected for a random alloy. The bars show the experimental distribution.

D. Discussion

To discuss the results for the growth of BGaN we will compare them to the well-known growth conditions for GaN grown by PAMBE. Figure 3.5 shows the growth map for GaN in PAMBE first described by Koblmüller *et al.*[26] overlaid with the growth conditions used in this experiment for all BGaN films. The growth condition used for the GaN buffer is provided as a reference. The BBr_3 flux is not represented in Figure 3.5 and was held constant for all films. This comparison to the growth map of GaN is used to frame the discussion. The evidence does not support a one to one correlation between the growth conditions of BGaN and GaN.

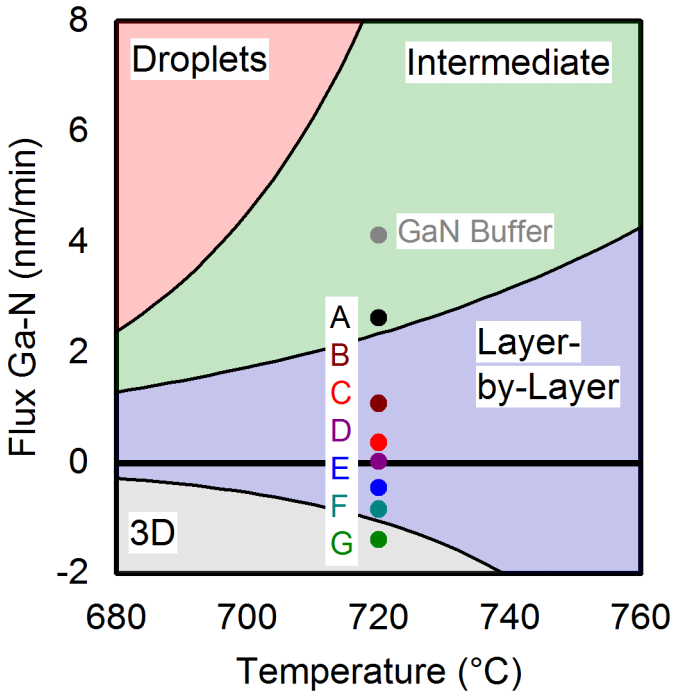

Figure 3.5 A growth map for PAMBE GaN based on research by Koblmüller et al.[26] The growth conditions for the BGaN samples and for the GaN buffer are overlaid, though B flux is not represented on the plot it is constant for all BGaN samples. The highest quality BGaN samples were grown in what corresponds to the layer-by-layer regime in GaN though all BGaN samples other than A had a 3D surface morphology.

At our growth temperature of 720 °C, there are four growth regimes for GaN as defined by Ga flux – active N flux. At highly N rich conditions, GaN films have a rough 3D surface and consequently it is called the 3D regime. At conditions where the Ga flux is similar to the N flux, the growth mode is layer-by-layer, this growth regime contains both Ga rich and N rich conditions. At conditions of significant Ga excess, a Ga adlayer greater than 1 ML forms. This intermediate regime with Ga adlayer between 1 ML and 2.4 ML is the target regime for modulated growth of GaN. With higher Ga flux the adlayer becomes greater than 2.4 ML and causes droplet formation and consequently is called the droplet regime.

During the growth of sample A, the RHEED dimmed and brightened in a manner that shows clear evidence of an adlayer. On the growth map, we see that by taking into account the Ga flux, we would expect the growth to be in an intermediate regime with a Ga adlayer greater than 1 ML but less than 2.4 ML, and consequently in a droplet-free regime. Sample A had no B incorporation and had droplets on the surface. Droplets on the surface indicate that the BBr_3 flux was in some way contributing the group III adlayer which pushed the net group III flux - active N flux into a droplet regime. The lack of B incorporation at this condition indicates that B is not incorporated on a "wet" Ga surface. This could originate from preferential incorporation of Ga over B or because the BBr_3 does not decompose under these conditions. The general trend is that elements with higher atomic number in the group III column incorporate more readily in III-nitride growth. Al incorporates preferentially to Ga which incorporates preferentially to In. However unlike AlN, GaN, and InN, BN is not stable in the wurtzite phase and this could explain why B might not follow this trend.

Samples B through F had high crystal quality and B incorporation which increased as Ga flux decreased. All of these samples were grown in conditions which based on the Ga flux

only, would be in a layer-by-layer regime with a Ga adlayer less than 1 ML. However, the RHEED did not show any evidence that the growth mode in this regime was layer-by-layer. Instead the RHEED for all samples showed a 3D surface. The only difference between samples B and C which were grown Ga rich and samples E and F which were grown N rich is the B composition which follows the general trend. This indicates that, similar to GaN, the growth regime for a slightly Ga rich and slightly N rich are similar.

Sample G has low crystal quality and according to the GaN growth map, was grown in conditions that correlate with low quality 3D growth. This does not necessarily mean that there is a different growth regime at this low Ga flux regime since all BGaN samples which shows B incorporation also had a 3D morphology. The low crystal quality of sample G could be caused by relaxation of the film or phase separation or both.

Despite the poor surface morphology, the RHEED and XRD both show evidence of high crystal quality in films B through F. In other III-nitride alloys, high quality films can be achieved with visible step edges on the surface which cannot be seen in BGaN on the AFM images. To the authors' knowledge, there have been no previous reports of BGaN films which show clear step edges on the surface. For PAMBE growth of GaN, it was found that a Ga adlayer greater than 1 ML is necessary to maintain good surface morphology at growth temperatures around 720 °C. However for BGaN we found that B did not incorporate with such an adlayer. This may be an experimental limitation of using BBr_3 as a B source rather than a material limitation. Different growth conditions may lead to better surface morphology.

Continuing studies will further explore the growth map for this material. In this paper the total growth time is controlled instead of the thickness. Due to the differences in growth

rates, this resulted in samples with different thicknesses. It should be possible if growth rates are calculated to grow samples of controllable thickness similar to standard group-III MBE. However, it has not been tested yet.

In this work we performed APT analysis on the highest B concentration sample that had high crystal quality in our series, to verify that it had a random alloy composition. This sample being a random alloy, the rest of the series which all had lower B concentration would also have a random alloy distribution. Random alloy distributions are important for electronic and photonic applications as it leads to consistent and predictable physical properties. Previous BGaN papers have not used APT to check for atoms distribution in 3D.

The APT analysis also agreed with the composition which we calculated from XRD analysis. The agreement between the independent measurements supports our theory that Vegard's law holds for wurtzite BGaN alloys. The XRD was simplified due to the fully strained nature of the films. The compositions cannot be directly solved using Vegard's law unless the unstrained lattice parameters are known. In this paper, we used the results from a density functional theory paper[7]. The agreement between the APT results and the XRD results calculated using the values from Dryer *et al.*[7] provide some experimental support for those wurtzite BN lattice parameter values.

Previous BGaN epitaxial layers have been grown primarily via MOCVD and resulted in films of lower crystal quality than those reported in this paper. Additionally previous reports have assumed that the grown films were fully relaxed, which is more likely for MOCVD growth where the temperature is high (> 900 °C) compared to PAMBE growth where the temperature is lower (720 °C). Our films may have a higher crystal quality

because they are not undergoing relaxation which would lead to the formation of crystal defects.

Future studies on BGaN will explore the effect of relaxation of the BGaN films and attempt to find the solubility limit of B in GaN at our growth conditions. This will help us determine if the decrease in crystal quality seen in films above 3.04% boron concentration was due to phase separation, relaxation induced defects or a combination of the two. Knowing this may help us modify the growth conditions to obtain samples with higher B concentrations.

E. Conclusion

We have demonstrated growth of high crystal quality BGaN films with compositions up to 3.04% grown coherently on GaN templated sapphire substrates using PAMBE. HRXRD experiments confirmed the high crystal quality of the films and the compositions of the films were calculated assuming Vegard's law using theoretical values for unstrained wurtzite phase BN. APT on the sample with the highest B concentration showed evidence of a random alloy distribution of group III elements indicating a good solid solution alloy. Finally, we demonstrated the first successful use of BBr_3 gas as a B source in III-nitride PAMBE.

Acknowledgements

Funded by a grant from the NSF Award No. DMR 1434854. Support for BB was provided by the Solid State Lighting and Energy Electronics Center (SSLEEC) at UCSB. Additional support for JSS was provided by ONR grant number N00014-15-1-2074. The MRL Central Facilities are supported by the MRSEC Program of the NSF under Award No. DMR 1121053; a member of the NSF-funded Materials Research Facilities Network (www.mrfn.org).

Chapter 3 References

[1] S. Nakamura, Solid State Commun. 102, 237 (1997).

[2] H. Masui, S. Nakamura, S.P. DenBaars, and U.K. Mishra, IEEE T. Electron Dev. 57, 88 (2010)

[3] M.T. Hardy, D.F. Feezell, S.P. DenBaars, and S. Nakamura, Mater. Today 14, 408 (2011)

[4] S. Nakamura, Thin Solid Films 343, 345 (1999).

[5] S. Rajan, P. Waltereit, C. Poblenz, S.J. Heikman, D.S. Green, J.S. Speck, and U.K. Mishra, IEEE Electr. Device L. 25, 247 (2004).

[6] U.K. Mishra, L. Shen, T.E. Kazior, and Y.F. Wu, P. IEEE 96, 287 (2008).

[7] C.E. Dreyer, J.L. Lyons, A. Janotti, and C.G. Van de Walle, Appl. Phys. Express 7, 031001 (2014).

[8] L. Guenineche and A. Hamdoune, Mater. Res. Express 3, 055003 (2016).

[9] C.H. Wei, Z.Y. Xie, J.H. Edgar, K.C. Zeng, J.Y. Lin, H.X. Jiang, J. Chaudhuri, C. Ignatiev, and D.N. Braski, J. Electron Mater. 29, 452 (2000).

[10] A.K. Polyakov, M. Shin, and M. Skowronski, J. Electron Mater. 26, 237 (1997).

[11] A. Kadys, J. Mickevičius, T. Malinauskas, J. Jurkevičius, M. Kolenda, S. Stanionytė, D. Dobrovolskas, and G. Tamulaitis, J. Phys. D: Appl. Phys. 48, 465307 (2015).

[12] T. Malinauskas, A. Kadys, S. Stanionytė, K. Badokas, J. Mickevičius, J. Jurkevičius, D. Dobrovolskas, and G. Tamulaitis, Phys. Status Solidi B, 252, 1138 (2015).

[13] T. Baghdadli, S. Ould Saad Hamady, S. Gautier, T. Moudakir, B. Benyoucef, and A. Ougazzaden, Phys. Status Solidi C 6, S1029 (2009).

[14] A. Ougazzaden, S. Gautier, C. Sartel, N. Maloufi, J. Martin, and F. Jomard, J. Cryst. Growth 298, 316 (2007).

[15] T.L Williamson, N.R. Weisse-Bernstein, and M.A. Hoffbauer, Phys. Status Solidi C 11, 462 (2014).

[16] D.S. Green, U.K. Mishra, and J.S. Speck, J. Appl. Phys. 95, 8456 (2004).

[17] C. Poblenz, P. Waltereit, and J.S. Speck, J Vac. Sci. Technol. B 23, 1379 (2005).

[18] K. Tamm, C. Mayeux, L. Sikk, J.F. Gal, and P. Burk, J. Mass. Spectrom. 341, 52 (2013).

[19] K. Thompson, D. Lawrence, D.J. Larson, J.D. Olson, T.F. Kelly, and B. Gorman, Ultramicroscopy 107, 131 (2007).

[20] T.J. Prosa, B.P. Geiser, D. Reinhard, Y. Chen, and D.J. Larson, Microsc. Microanal. 22, 664 (2016).

[21] B. Heying, R. Averbeck, L.F. Chen, E. Haus, H. Riechert, and J.S. Speck, J. Appl. Phys. 88 1855 (2000).

[22] A.R. Denton, N.W. Ashcroft, Phys. Rev. A 43, 3161 (1991).

[23] M. Leszczynski, H. Teisseyre, T. Suski, I. Grzegory, M. Bockowski, J. Jun, S. Porowski, K. Pakula, J.M. Baranowski, C.T. Foxon, and T.S. Cheng, Appl. Phys. Lett. 69, 73 (1996).

[24] A.F. Wright, J. Appl. Phys. 82, 2833 (1997).

[25] M.P. Moody, L.T. Stephenson, A.V. Ceguerra, and S.P. Ringer, Microsc. Res. Techniq. 71, 542 (2008).

[26] G. Koblmüller, S. Fernández-Garrido, E. Calleja, and J.S. Speck, Appl. Phys. Lett. 91, 161904 (2007).

Chapter 4: BBr_3 as a boron source in plasma-assisted MBE

Boron is a difficult material to use in a molecular beam epitaxy (MBE) reactor due to its high melting point as a pure compound. Consequently, there is interest in exploring alternative sources for B in MBE. In this paper we detail the construction and operation of a novel BBr_3 injection system for plasma-assisted MBE growth and show results for BGaN thin films grown using readily available low purity BBr_3 as a proof of concept for the source. The BBr_3 system enables the growth of coherent BGaN films with concentration up to 3% B on the group III site and thicknesses up to 280 nm as determined by high resolution X-ray diffraction. Atom probe tomography and secondary ion mass spectroscopy results of a $B_{0.03}Ga_{0.97}N$ film indicate a high level of Br impurity on the order of 1×10^{19} atoms/cm^3 and atmospheric contamination consistent with a low purity source. BBr_3 is successful as a B source for high crystal quality BGaN films however the Br incorporation from the source limits the applications for this material. This work is reprinted with permission from the Journal of Vacuum Science and Technology A [BBr_3 gas as a boron source in plasma-assisted molecular beam epitaxy, Richard C. Cramer, Bastien Bonef, and James S. Speck, *Journal of Vacuum Science and Technology A* In Press (2019)]

A. Introduction

In molecular beam epitaxy (MBE) many metallic sources are converted into molecular beams by evaporating or sublimating pure metals at high temperature. For materials that constitute the bulk of an epitaxial film (as opposed to dopants) this temperature is generally hundreds of degrees above the melting point of the metal. For materials with high melting points such as B (melting point = 2076 °C[1]) the temperatures required to get significant sublimation rates are higher than the operating temperatures of the crucibles for traditional effusion cells. Experimental high temperature crucibles exist[2] that can reach temperatures of ~2100 °C but even at these elevated temperatures B fluxes would be low compared to other group III sources. Beyond effusion cells, other options to grow using these elements include electron beam[3] and gas sources.[4] In this paper we present a technique to use BBr_3 gas as the B source in plasma-assisted MBE. As a proof of concept for this method, we demonstrate the growth of high crystal quality BGaN thin films.

In previous reports[5] we demonstrated high crystal quality growth of coherent ~100 nm $B_xGa_{1-x}N$ films over a range of compositions from 1-3% B on the group III site using BBr_3 as the B source. Additionally we showed that the films had a random alloy distribution of B and Ga atoms using atom probe tomography (APT).[6] In this paper we explain in detail our BBr_3 injection systems construction and operation, we present the coherent growth of a 280 nm thick $B_{0.03}Ga_{0.97}N$ layer, and we discuss secondary ion mass spectroscopy (SIMS) and APT results that show the current limits of our BBr_3 source as it applies to BGaN. The primary limitation for BGaN is high levels of Br impurities in the films which may be a fundamental limitation of the BBr_3 source.

BBr_3 is a liquid at room temperature and pressure and is easily vaporized at lower pressures and/or elevated temperatures. To inject BBr_3 gas into the MBE chamber a custom system was built and will be described in detail in the experimental section of this report. A BBr_3 source was selected due to the previous success of CBr_4 used as a gas source for C doping of GaN in plasma assisted MBE.[7] It is believed that in the CBr_4 doping of GaN the CBr_4 decomposes on the growing GaN surface and thus creates elemental C which readily incorporates into the film. SIMS results indicate that when using CBr_4 to dope GaN with a target C concentrations in the 10^{16} cm^{-3} to 10^{18} cm^{-3} range Br was unmeasurable and presumably desorbs as Br_2 during the growth process.[7] To achieve alloying levels of B from our BBr_3 source we need four orders of magnitude higher gas flux than in the CBr_4 experiments. As we will show this leads to Br incorporation which is not seen in CBr_4 doped GaN films.

The group III-nitride system (AlN, GaN, InN, and their alloys) has demonstrated applications in light emitting diodes,[8, 9] laser diodes,[10, 11] and high frequency power electronics[12, 13] and can be grown via common high quality epitaxial growth technique including MOCVD[14] and MBE.[15] Due to its demonstrated utility, there is interest in expanding this materials system to include the alloys with BN such as BGaN and BAlN. There have been theoretical predictions for the potential properties of BGaN[16] and BAlN[17] and confirming or refuting these predictions would be of great interest for the materials community for making future predictions of similar extreme alloy systems. Wurtzite phase BN is unstable but density functional theory calculations predict that if it were to exist it would have small (compared to AlN) lattice constants, a = 2.52 Å, c = 4.17 Å, as well as a wide band gap, 10.13 eV direct gap, 6.46 eV indirect gap.[18] Determining the material properties of wurtzite phase BGaN or

BAlN alloys would be interesting to see if Vergard's Law holds when one of the end points can only be predicted by theory. Additionally, the high band gap of the materials would make BAlN potentially useful for deep UV optoelectronic applications if high quality, low impurity material could be grown.

B. Experimental

The BBr_3 gas for this experiment and the previous results[5, 6] was injected into the MBE using a custom built system as shown schematically in Fig. 4.1. The BBr_3 liquid is held in our custom bubbler (Fig. 4.1a). The bubbler has a load cap, a single outlet line, and is mounted with a thermoelectric temperature controller which allows the bubbler temperature to be held in a range from -20 °C to 30 °C. Over this temperature range the vapor pressure of the BBr_3 changes by almost two orders of magnitude.[18] The outlet line of the bubbler goes through a variable leak valve (Fig. 4.1b) then either a 1 mm^2 conductive orifice or through both the 1 mm^2 orifice and a full 18.3 mm^2 diameter tube (Fig. 4.1c). Finally the gas is injected into the Varian Gen II MBE system through a tube positioned around the straight-on pyrometer viewport (Fig. 4.1d). The inner tube is a viewport for infrared pyrometry measurements of the substrate during growth and the BBr_3 gas flows through the outer tube. Inside the MBE system the injection tube has a multi-hole nozzle designed to evenly spread the gas flux (Fig. 4.1e). The injection nozzle has 40, 0.6 mm^2, holes evenly spaced in a circle with a radius of 2.54 cm. 36 holes were drilled with a 4° outward angle while a set of four holes set every 90 degrees have an 8° degree inward angle. The 1:6 diameter to length ratio for the holes combined with the angling of the holes is predicted to facilitate an even spreading of the gas flux over a 2 inch wafer at a distance between the nozzle and substrate of 9.4 cm. The injection system also has an ion pump (Fig. 4.1f) used to pump the system down to 10^{-8} Torr when not in use and to redirect the gas flow into once established (see below).

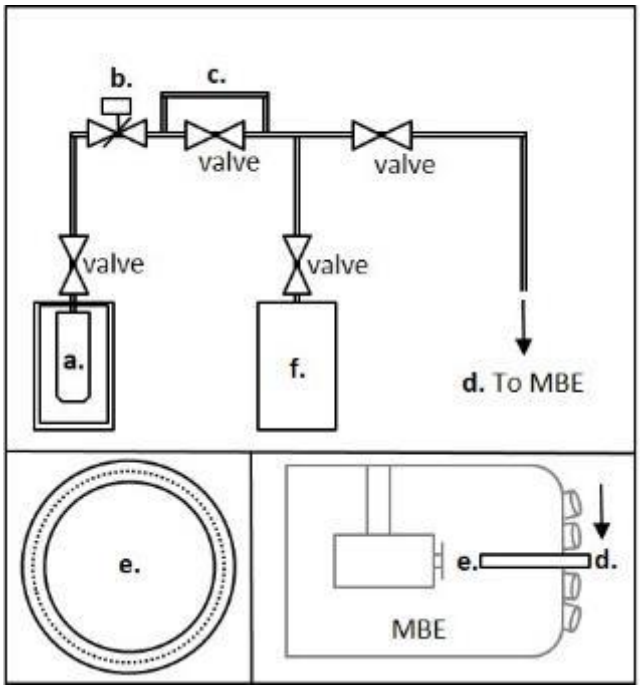

Figure 4.1. Schematic of the BBr_3 Injection System
(a.) BBr_3 bubbler with thermoelectric temperature control. (b.) variable leak valve (c.) low flux 1 mm^2 orrifice and valve which opens an optional 18.3 mm^2 orrafice (d.) injection tube to MBE system. (e.) nozzle side of the injection tube (f.) ion pump.

The amount of BBr_3 gas flowing into the system was qualitatively measured using a beam flux monitor (BFM) which is a Bayard-Alpert Gauge positioned at the growth position in the MBE chamber. Although the BFM provides a pressure value, it requires a specific calibration for each gas species to be accurate. Such a calibration is unavailable for BBr_3. Consequently, the conversion from pressure as measured by the BFM to an absolute molecular flux is non-trivial and the beam equivalent pressure may vary between machines. The three flow control mechanisms of temperature, leak valve, and choice of orifice gave us a useable range of BBr_3 flows from below the detection limit of the BFM (10^{-11} Torr) to ~10^{-5} Torr. Experimentally we found BBr_3 fluxes useful for BGaN growth to be in the range of 10^{-8} Torr to 10^{-6} Torr. The set of fluxes obtained by varying the temperature of the bubbler while holding the leak valve position constant at halfway open and the bypass valve closed are displayed in Fig. 4.2.

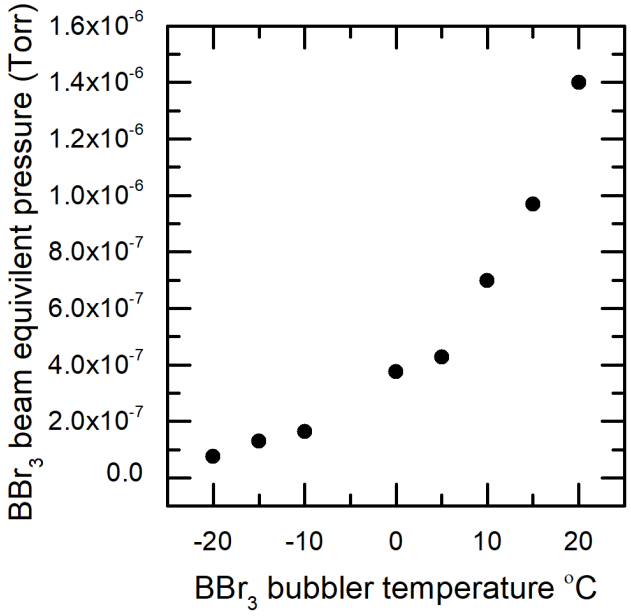

Figure 4.2. BBr_3 Beam Equivalent Pressure
BBr_3 beam equivalent pressure as a function of bubbler temperature with the leak valve held at a constant midway open position and the bypass valve closed.

The BBr_3 liquid as received from the supplier (STREM 5N purity) was poured into our custom bubbler under an inert high purity nitrogen atmosphere. Note that 5N purity is two orders of magnitude less pure than our other sources for MBE however it was the most pure material that was readily available for this proof of concept experiment. The bubbler was placed within the injection system and the rest of the system was put through a standard purge/pump cycle; filled with N_2 gas then pumped down to a pressure of 1 x 10^{-7} Torr three times then baked at 100 °C for 4 hours. This purge, pump, bake process was used to drive air and water out of the system prior to flowing BBr_3 gas. To remove the N_2 gas in the BBr_3 source bubbler, it was cooled to -20 °C and opened to a roughing scroll pump to pull off the N_2 while leaving most of the BBr_3 in a liquid state. After the majority of the N_2 was pumped out of the

bubbler, we established a BBr_3 flow to the MBE system where we confirmed that the partial pressure of N_2 introduced into the system with the BBr_3 was below 1×10^{-9} Torr using a quadrupole mass spectrometer mounted within the MBE growth chamber (RGA 200, Stanford Research Systems).

Prior to each growth, the flux of BBr_3 in the MBE system was measured using the BFM and any necessary adjustments to BBr_3 temperature or leak valve position were made. Since the injection system was kept in vacuum when not in use, on the first growth of a day it could take up to 10 minutes to establish a constant flux in the MBE as the gas slowly moved through the injection system. Once the target flux was established the valve to the main MBE chamber (Fig. 4.1d) was closed and the valve to the ion pump (Fig. 4.1f) was opened redirecting the gas flow from the main chamber into the ion pump. With the flow redirected into the ion pump instead of stopped such that the desired BBr_3 flux could be reestablished on a time scale of ~30 seconds as opposed to 10 minutes.

200 - 300 nm thick samples of $B_xGa_{1-x}N$ were grown on a GaN on-sapphire substrates with $x = 0.02 - 0.03$. Prior to growth, the back side of the sapphire substrates were coated with 500 nm of Ti to act as an absorbing material for the IR heating and as an IR emitter for pyrometry. The film was grown at 720 °C for 45 min of total growth time under slightly group III rich conditions. We used a technique of modulated growth where the growth was performed in nine 5 min periods with 30 s growth interrupts to allow excess Ga to desorb.[19] The active nitrogen was provided by a Riber RFN-50/63 nitrogen plasma source equipped with an auto-tuning unit and operated with 3 sccm of high purity N_2 and 200 W of RF power. The Ga flux was provided by a traditional effusion cell operated at temperatures that corresponds to beam pressures in the range of 5.3×10^{-7} to 7.3×10^{-7} Torr as measured by the

BFM. Boron was provided by a flow of BBr_3 gas which had a BFM pressure of 5.90×10^{-7} Torr. The growth techniques used in this paper are the same as those presented in a previous paper.[7]

To analyze the crystal quality and composition of the films we used high resolution X-ray direction (HRXRD) on a Philips Panalytical MRD PRO diffractometer with a four bounce Ge (220) monochromater using Cu-$K_{\alpha 1}$ incident radiation (λ = 1.5405 Å). The signal was collected using a sealed proportional counter detector and a two bounce Ge (220) analyzer crystal. We measured 0002 peaks in an ω-2θ geometry. We also performed reciprocal space maps around the $\bar{1}015$ reflection in an asymmetric geometry to verify if the films were fully coherent with the underlying GaN template.

To measure the Br impurity levels, 300 nm thick films of $B_{0.02}Ga_{0.98}N$ and $B_{0.03}Ga_{0.97}N$ were grown with 200 nm GaN caps and the Br concentration as a function of depth was measured via SIMS (EAG Laboratories).

To investigate the atomic distribution of B, O and C in a $B_{0.03}Ga_{0.97}N$ layer, the sample was investigated using APT. A 200 nm GaN cap was re-grown on top of the BGaN layer to facilitate the preparation of the APT thin needle by focused ion beam (FIB). An FEI Helios 600 dual beam FIB instrument was used for the preparation following standard procedure with final Ga beam energy reduced to 2 keV to minimize FIB damage. The APT analysis was performed with a Cameca 3000X HR Local Electrode Atom Probe (LEAP) operated in laser-pulse mode (13 ps pulse, 532 nm green laser, 10 µm laser spot size) with a base temperature of 45 K. The laser pulse energy and the detection rate for the experiments were respectively set to 1 nJ and 0.005 atoms per pulse for reliable quantification of B.[6] APT 3D reconstruction

was carried out using commercial software IVAS^{TM} and by using the thickness of the BGaN layer determined by XRD as a reference.

To determine the oxygen concentration in our BGaN films we grew samples of GaN and $Al_{0.03}Ga_{0.97}N$ at comparable growth conditions (as a check on unintentional oxygen concentration in our MBE fimls), 720 °C and a near stoichiometric ratio of group III and N fluxes. The oxygen and carbon concentration in these samples was measured via SIMS (Cameca IMS 7f Auto SIMS).

C. Results

The 0002 ω-2θ scan HRXRD scan of a representative $B_{0.02}Ga_{0.97}N$ film can be seen in Fig. 4.3a. Thickness fringes can be seen indicating high crystal quality and enabling us to determine the film thickness from the angular spacing of the fringes. Consistent with our previous reports, the reciprocal space map around the $\bar{1}015$ peak (Fig. 4.3b), shows the lower intensity film peak to same in-plane component of the peak as the GaN template peak, thus demonstrating that the film is fully coherent. We calculated the B content of the films using Vegard's Law, theoretical literature values for the lattice constants of wurtzite phase BN, and using the elastic parameters of GaN to predict the deformation due to being strained to the substrate. The method is explained in detail in a previous work.[5] It is worth noting that this film is coherent at a thickness of 280 nm. The critical thickness for stress relaxation by cracking or dislocation formation is a topic of ongoing investigation for BGaN films.

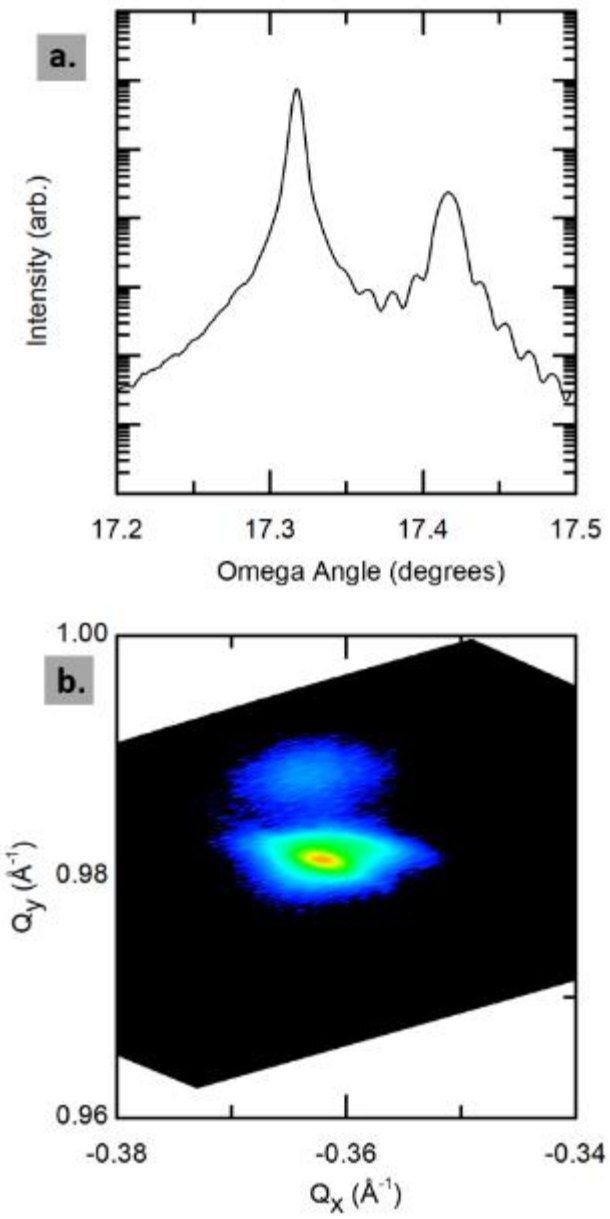

Figure 4.3 (XRD results
(a.) a 0002 XRD scan of a 280 nm $B_{0.02}Ga_{0.98}N$ thin film grown on a GaN template on sapphire substrate (b.) a RSM around the $\bar{1}015$ peaks for the substrate and, above it, the BGaN film.

The SIMS results for a $B_{0.02}Ga_{0.98}N$ film show a peack Br concentration on the order of 2 x 10^{18} cm^{-3}, the results for the $B_{0.03}Ga_{0.97}N$ film show that the Br concentration is on the order of 1 x 10^{19} cm^{-3} at its highest point (Fig. 4.4). Although high levels of Br were measured in the BGaN layer the Br concentration in the surrounding GaN layers was below the SIMS detection limit of ~10^{15} cm^{-3}. We do not see sharp changes of Br concentration at interfaces of the BGaN layer and we see a Br concentration peak at the initial growth interface (~800 nm), this is most likely due to residual BBr_3 in the MBE from the flux check performed ~1 hour before growth. While it is not explored in this study, Br doping at that level would likely strongly impact the electrical properties of a BGaN film grown using BBr_3.

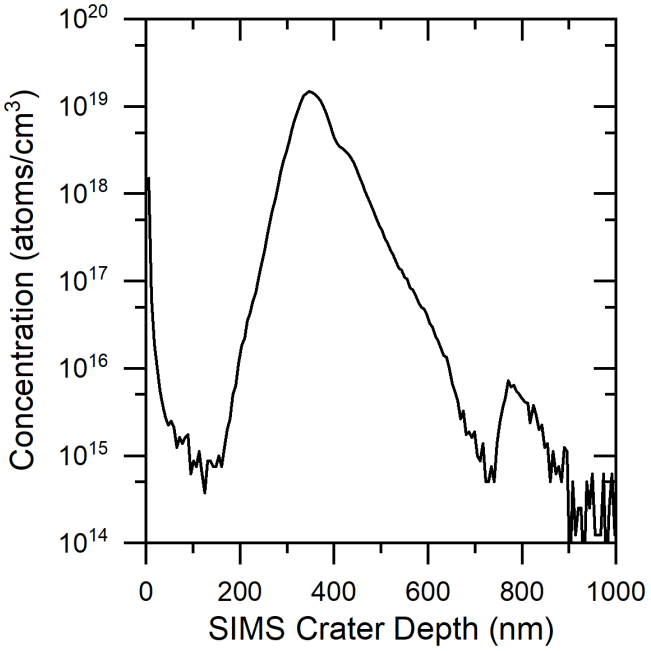

Figure 4.4 SIMS Results.
Br depth profile of a 300 nm thick $B_{0.03}Ga_{0.97}N$ film with a 200 nm UID GaN cap on a 300 nm thick GaN buffer layer. The BGaN layer is located between 200 nm and 500 nm and the MBE growth/substrate interface is at 800 nm.

Fig. 4.5a shows a 1D concentration profile measured from the APT volume obtained on a $B_{0.03}Ga_{0.97}N$ sample. The B level as measured by APT (1.8×10^{21} cm^{-3}) is in approximate agreement to the concentration as determined via XRD ($B_{0.03}Ga_{0.97}N$ would have a B concentration of 1.3×10^{21} cm^{-3}). There is an elevated level of B in the GaN cap which indicates that after we turn off the deliberate BBr_3 flow there is residual BBr_3 in the growth chamber that incorporates into the film. The BBr_3 source does not have a shutter, only a valve external to the MBE, this prevents us from having an instantaneous cut-off of the gas flow.

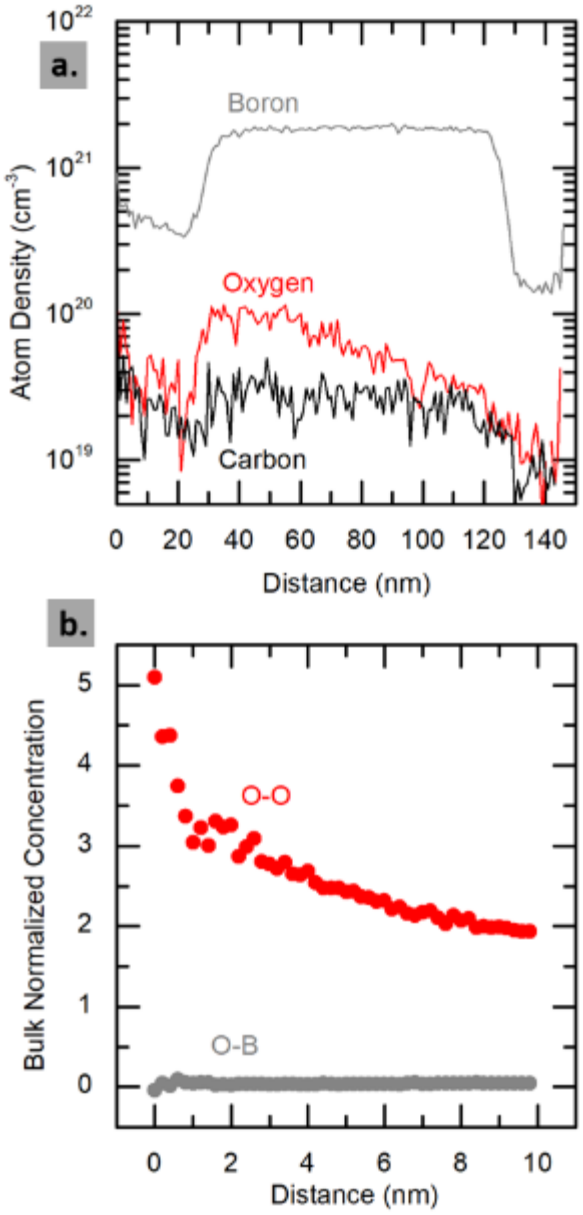

Figure 4.5 APT results
(a.) B, O, and C depth profile of a $B_{0.03}Ga_{0.97}N$ film with a GaN cap. (b.) A radial distribution analysis which shows that O is likely to cluster with other O atoms but does not correlate with B atoms.

Also in Fig. 4.5a, C and O signals can be clearly observed in the BGaN layer. C and O peaks in the APT mass spectrum are not observed in the GaN top and bottom layers which indicate that their presence in these layers are below the detection limit of APT. For the $B_{0.03}Ga_{0.97}N$ sample (Fig. 4.5a), C impurities are 3.0 x 10^{19} cm^{-3} while O impurities are 9.9 x 10^{19} cm^{-3}. In the APT mass spectrum Br was not detected however based on our SIMS results we expect it to be of order 1.0 x 10^{19} cm^{-3} which is around the noise level for this APT analysis.

The respective distribution of O and B in the BGaN layer was studied using the radial distribution analysis (RDA) method. The ratio of the composition found in spherical shells around each O atoms to the overall sample composition is plotted versus the shell radius (Fig. 4.5b). A self O-O correlation curve was generated by measuring the compositions of O. A cross O-B correlation curve was generated by measuring the compositions of B. Ratios above one in these two curves would respectively indicate O-O or an O-B affinities. Here, only O rich regions were detected in the BGaN layer which do not correspond to a local increase in the B concentration since the O-B cross correlation curve remains constant around one. O incorporation in the BGaN layer is not favored by the presence of B locally during growth. Similar statistical analysis were performed for C but its low content level in the sample prevented us from getting a reliable distribution a short scale.

SIMS results for the GaN and $Al_{0.03}Ga_{0.97}N$ films grown under comparable growth conditions found O levels of 5 x 10^{16} cm^{-3} and 1 x 10^{17} cm^{-3} respectively and C levels of 2 x 10^{16} cm^{-3} for both. The low O concentration in the GaN film shows that the MBE system used in this study has low overall oxygen impurities. The O concentration in the AlGaN sample are higher than the GaN as is expected however they are still significantly lower than the BGaN sample.

D. Discussion

The BBr_3 source has been used successfully to grow BGaN films with reliable and reproducible results. The HRXRD results show that the system can grow high crystal quality samples. However the high levels of O and Br impurities in the current samples make measuring the electrical properties of BGaN challenging.

The growth conditions at which we found B to incorporate into a GaN film (720 °C, N-rich) are known to lead to increased O uptake when compared to hotter or more Ga rich MBE growth of GaN.[20, 21] However the control sample of $Al_{0.03}Ga_{0.97}N$ grown in our MBE chamber at comparable growth conditions had a peak O concentration of 1 $x10^{17}$ cm^{-3} and a C concentration of 2 x 10^{16} cm^{-3} compared to 9.9 $x10^{19}$ cm^{-3} O and 3.0 $x10^{19}$ cm^{-3} C for the $B_{0.03}Ga_{0.97}N$ films. This leads to the conclusion that it is not the growth condition or the MBE chamber leading to the O and C impurities but the BBr_3 source itself.

The BBr_3 gas as received is 5N purity which is significantly lower than the other material inputs in our MBE. The Ga used in our MBE system is 7N purity (UMC Corp). The N_2 used for our nitrogen plasma is 6N purity (Matheson) and passes through two sequential purifiers (SAES MC1-902F) before flowing into the plasma cavity. Higher purity sources of BBr_3 are available (Versum Materials 6N8 purity/99.99998%) as it is used as a B source for thermal diffusion doping of Si[22, 23] however due to the cost and the difficulty of acquiring research quantities of the high purity reagent a less pure, more readily available source was selected for this proof of concept study.

Based on source material purity alone if O and B incorporated into the films at the same rate we would expect to see six orders of magnitude less O than B instead we only see one order of magnitude difference. We know that O incorporation is high at this growth condition

and that B incorporation into the film requires BBr_3 to decompose first which may lower the incorporation efficiency of BBr_3 compared to a pure B source. However combining these factors it is still unlikely that we would get such high O levels with a 5N purity source so we speculate that our BBr_3 material entering the MBE is less pure. This is either due to contamination at some point in the materials handling process or an undetected leak in our BBr_3 injection system. In the absence of such factors we expect the O and C concentrations to be significantly lower.

The Br contamination is a more concerning issue for this growth method since using BBr_3 as a B source for BGaN films appears to inevitably result in a large unintentional Br incorporation. While it is clear that B incorporates preferentially to Br, the Br incorporation is high. For the growth of $B_{0.02}Ga_{0.98}N$, B is incorporating ~1800 times more readily than Br while for the growth of the $B_{0.03}Ga_{0.97}N$ film the B incorporated only ~360 times more readily than Br. Both samples had the same BBr_3 and N fluxes into the chamber but had different Ga fluxes and therefore different B and Br incorporation rates. It is still unclear on what type of dopant Br would be in a III-nitride compound but as a halogen it is likely electrically active. It is possible that changing growth conditions could lower the Br incorporation. However, unlike O incorporation which we can compare with analogous materials, such systems are not available yet for Br incorporation. Consequently, predicting Br incorporation behavior is not possible for now. We believe this to be the largest barrier to implementing BBr_3 as a B source for BGaN films.

E. Conclusion

The technique we developed to use BBr_3 as a B source in plasma-assisted molecular beam epitaxy growth of III-nitride films is successful for growing high crystal quality films $B_{0.02}Ga_{0.97}N$ films coherently up to 280 nm thick. This growth condition is 720 °C with an excess of N. The B content of the films is controlled by varying the Ga and BBr_3 fluxes. Unfortunately for BGaN the BBr_3 source also leads to a high level of Br impurities which makes BBr_3 an infeasible source for BGaN devices. The high crystal quality of the films and the ability to control the B concentration indicates that the BBr_3 source may be useful for other B containing materials that incorporate Br less readily such as BN.

Acknowledgements

Funded by a grant from the NSF Award No. DMR 1434854. Support for BB was provided by the Solid State Lighting and Energy Electronics Center (SSLEEC) at UCSB. Additional support for JSS was provided by ONR grant number N00014-15-1-2074. The MRL Central Facilities are supported by the MRSEC Program of the NSF under Award No. DMR 1121053; a member of the NSF-funded Materials Research Facilities Network (www.mrfn.org).

Chapter 4 References

[1] Los Alamos National Laboratory Periodic Table, “periodic.lanl.gov”

[2] K. Eberl, High Temperature Effusion Cell HTEZ, “www.mbe-komponenten.de”

[3] Laleyan D.A., Mengle, K., Zhao, S., Wang, Y., Kioupakis, E., and Mi, Z. Opt. Express **26**, 23031 (2018)

[4] X. Wang, M. Hossain, Z. Wei, and L. Xie. Nanotechnology. **30**, 034003 (2019)

[5] R.C. Cramer, B. Bonef, J. English, C.E. Dreyer, C.G. Van de Walle, and J. S. Speck, J. Vac. Sci. Technol. A **35**, 041509 (2017)

[6] B. Bonef, R. Cramer, J.S. Speck, and J. Appl. Phys. **121**, 225701 (2017)

[7] D.S. Green, U.K. Mishra, and J.S. Speck, J. Appl. Phys. **95**, 8456 (2004).

[8] S. Nakamura, Solid State Commun. **102**, 237 (1997).

[9] H. Masui, S. Nakamura, S.P. DenBaars, and U.K. Mishra, IEEE T. Electron Dev. **57**, 88 (2010)

[10] M.T. Hardy, D.F. Feezell, S.P. DenBaars, and S. Nakamura, Mater. Today **14**, 408 (2011)

[11] S. Nakamura, Thin Solid Films **343**, 345 (1999).

[12] S. Rajan, P. Waltereit, C. Poblenz, S.J. Heikman, D.S. Green, J.S. Speck, and U.K. Mishra, IEEE Electr. Device L. **25**, 247 (2004).

[13] U.K. Mishra, L. Shen, T.E. Kazior, and Y.F. Wu, P. IEEE **96**, 287 (2008).

[14] D.F. Brown, S. Keller, T.E. Mates, J.S. Speck, S.P. DenBaars, and U.K. Mishra, J. Appl. Phys. **107**, 033509 (2010)

[15] E.C.H. Kyle, S.W. Kaun, F. Wu, B. Bonef, and J.S. Speck, J. Cryst. Growth **454**, 164 (2016).

[16] C.E. Dreyer, J.L. Lyons, A. Janotti, and C.G. Van de Walle, Appl. Phys. Lett. **7**, 031001 (2014)

[17] J.X. Shen, D. Wickramarantne, and C.G. Van de Walle, Phys. Rev. Materials **1**, 065001 (2017)

[18] Versum Materials LLc, BORON TRIBROMIDE (BBr3) 325-12-101-GLOBAL, "https://www.versummaterials.com/product/boron-tribromide-extrema" (2016)

[19] C. Poblenz, P. Waltereit, and J.S. Speck, J. Vac. Sci. Technol. B **23**, 1379 (2005)

[20] G. Koblmüller, R. M. Chu, A. Raman, U. K. Mishra, and J. S. Speck, J. Appl. Phys. **107**, 043517 (2010)

[21] C.R. Elsass, T. Mates, B. Heying, C. Poblenz, P. Fini, and P. M. Petroff, Appl. Phys. Lett. **77**, 3167 (2000)

[22] P. Negrini, A. Ravaglia, and S. Solmi, J. Electrochem. Soc. **125**, 609 (1978)

[23] M. Miyoshi, N. Shimizu, Y. Imanishi, O. Oda, and J. Nishizama, J. Electrochem. Soc. **152**, G601. (2005)

Chapter 5: Demonstration of BAlN and h-BN via plasma-assisted MBE

A. Proof of concept: BAlN

In Chapters 3 and 4 we presented initial results for the growth of BGaN via MBE using BBr_3 as a B source. BGaN is interesting as it represents a novel extreme alloy but also due to its potential for having a high band gap and large polarization charge density. BAlN is interesting for the same reasons. We do not have enough data to present a thorough study of the growth of BAlN via MBE but we can present data of a proof of concept for the growth of BAlN using the BBr_3 source.

Using comparable growth conditions those that resulted in a $B_{0.03}Ga_{0.97}N$ film a thick BAlN film was grown. Nitrogen plasma of 1 sccm 300 W which corresponds to an AlN equivalent growth rate of ~4 nm/min, BBr_3 flux of 3.60 x 10^{-7} Torr, and an Al flux of 5.05 x 10^{-8} Torr which corresponds to an AlN equivalent growth rate of ~2.5 nm/min. 120 minutes total growth time with a constant substrate temperature of 720 °C. The substrate for this experiment was 4H-SiC (Cree) which had a thick MOCVD AlN buffer layer. Prior to growth, 500 nm of Ti was deposited onto the back of the SiC to serve as an IR absorber for heating and an IR emitter for IR pyrometry. The emissivity for the Ti backed SiC substrate was calibrated via the melting point of Al.

A high resolution X-ray diffraction (XRD) scan of the sample can be seen in Figure 5.1. The 0002 on axis peak (Fig. 5.1a) shows the SiC substrate peak on the far left, the central

AlN peak, and to the right the BAlN peak. The thickness fringes of the BAlN peak were used to determine film thickness of 236 nm and are indicative of good crystal quality. The reciprocal space map around the off axis $\bar{1}015$ peak (Fig. 5.1b) show that the BAlN peak is directly above the AlN peak in reciprocal space indicating that the BAlN is fully strained to the AlN.

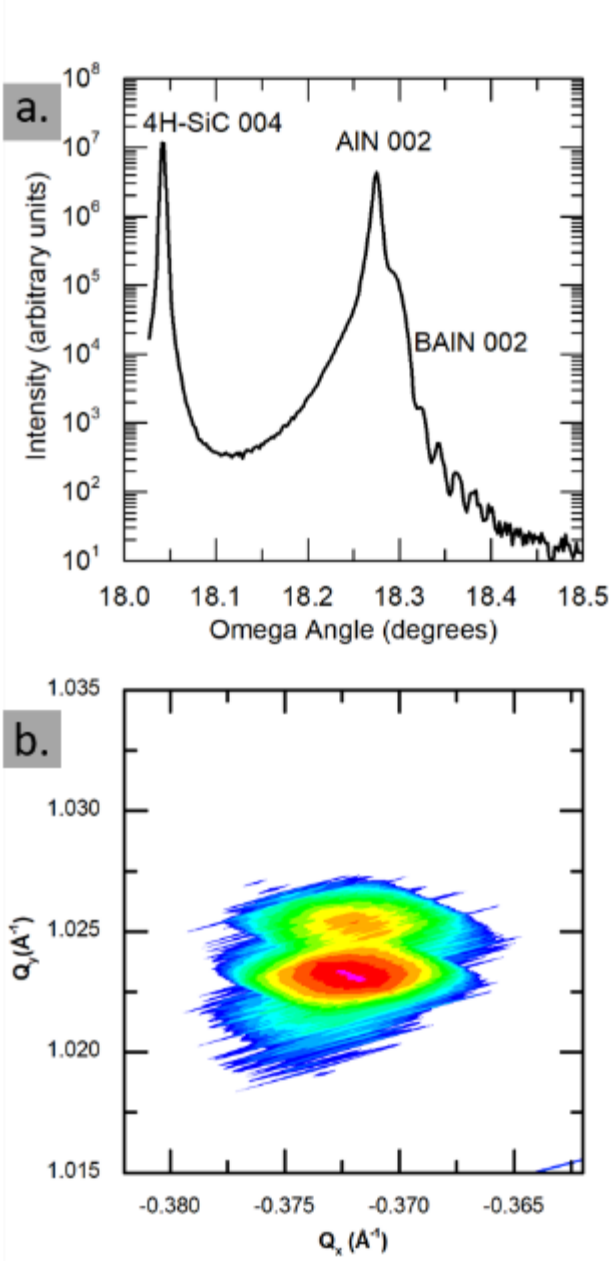

Figure 5.1 BAlN XRD
(a.) On axis omega two-theta scan: 0004 SiC substrate peak on the far left, 0002 AlN peak in the middle and 0002 BAlN peak with fringes on the right side of the AlN peak. (b.) Reciprocal space map around the $(\bar{1}015)$ peak for AlN. The BAlN peak is directly above the AlN peak which means the BAlN film is fully strained to the AlN layer.

To calculate the composition of the BAlN film we determined its strained c parameter (c_{BAlN}) from the 0002 omega-two theta scan using Bragg's Law and the 0004 4H-SiC substrate peak as a reference point. Based on the RSM we know that the BAlN is fully coherent to the underlying AlN and therefore $a_{AlN,o} = a_{BAlN.}$ Using standard stress-strain relations, the elastic properties of AlN (C_{13} & C_{33}), and literature values for the lattice constants of relaxed AlN ($a_{AlN,\,o}$ and $c_{AlN,\,o}$)[1] and wurtzite phase BN ($a_{BN,\,o}$ and $c_{BN,\,o}$). We calculated the strained composition x of the BAlN by solving the following system of equations.

$$c_{BAlN,o} = c_{BN,o}(x) + (1-x)c_{AlN,o} \tag{5.1}$$

$$a_{BAlN,o} = a_{BN,o}(x) + (1-x)a_{AlN,o} \tag{5.2}$$

$$\left(\frac{c_{BAlN} - aB_{AlN,o}}{a_{BAlN,o}}\right) = -\left(\frac{2\,C_{13}}{C_{33}}\right)\left(\frac{a_{AlN,o} - a_{BAlN,o}}{a_{BAlN,o}}\right) \tag{5.3}$$

Where $c_{BAlN,o}$ and $a_{BAlNo,}$ are the relaxed lattice constants for a BAlN film of compositions x. From this analysis we calculated the composition to be approximately 5% B on the group III site. This measurement is somewhat complicated by the broad AlN peak which overlaps a significant portion of the BAlN peak. The broad AlN peak is a result of the varied strain states which results from heteroepitaxy of AlN on SiC.

A second sample was prepared using the same growth conditions as the previous sample with an additional 200 nm AlN cap grown on top using the same N flux and an Al flux of

1.16 x 10^{-7} Torr beam equivalent pressure. Atom probe tomography (APT) was performed by collaborator Dr. Bonef. The APT results gave a composition of 6% B on the group III site in rough agreement with our XRD results but also indicated that there was significant clustering of the B within the film and it was not a pure random alloy. A comparison of the observed concentration distribution with a purely random binomial distribution is displayed below in Figure 5.2.

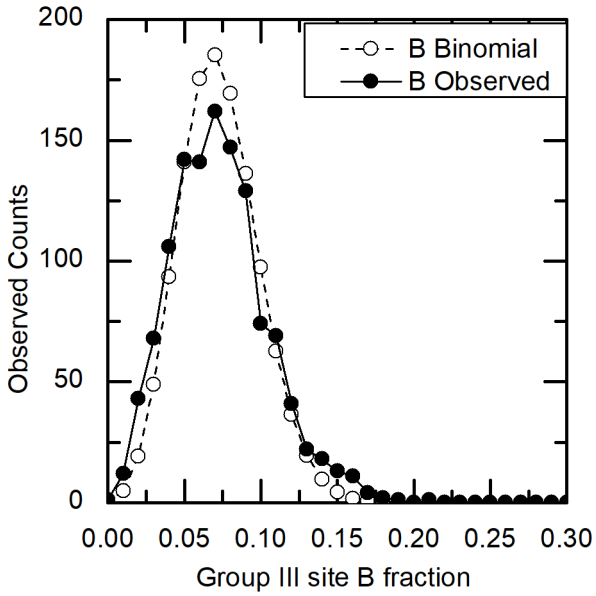

Figure 5.2 Boron distribution in BAlN vs binomial distribution
The distribution of B within the ~5% BAlN film. Note that the B distribution (closed circles) is broader and shallower than a binomial distribution (open circles) which is indicative of clustering within the film rather than a random alloy.

Comparing the BAlN growth to our previous work on BGaN[2, 3] it is noteworthy that comparable growth conditions lead to increased B incorporation. Due to the chemical similarity between B and AlN and the lower lattice mismatch between wurtzite BN and AlN this is not unexpected. These initial results are promising and demonstrate that the BBr_3

source works for BAlN as well as BGaN. However the Br incorporation that was observed in the BGaN is likely to be a problem in BAlN films as well. Additionally we have not yet demonstrated a random BAlN alloy. Due to time constraints this work will not be completed by the author but may serve as a starting point for a future graduate student.

B. Proof of concept: hexagonal BN

Hexagonal boron nitride is an interesting material particularly to the 2D physics and electronics communities.[4, 5, 6] While it is not an extreme alloy testing if our experimental BBr_3 could be used to grow BN was a natural experiment to perform.

We deposited a film using a BBr_3 flux of 3.60×10^{-7} Torr, a nitrogen plasma of 1 sccm flow of N_2 and 300 w of plasma power for a total growth time of 90 minutes at a growth temperature of 730 °C. The substrate for this growth was 4H-SiC (Cree) which has undergone chemical mechanical planarization to have unit cell step height. Prior to growth 500 nm of Ti was deposited onto the back of the SiC to serve as an IR absorber for heating and an IR emitter for IR pyrometry. The emissivity for the Ti backed SiC substrate was calibrated via the melting point of Al.

Measuring h-BN via XRD is particularly difficult since the low Z ratio of the B atoms results in low intensity XRD reflections. Using a significantly higher integration time than our other XRD scans we did manage to see evidence that we had h-BN deposited on the film as can be seen in Figure 5.3. This initial study of h-BN grown using BBr_3 source is far from conclusive however it does show enough promise that it may be of interest for future research. The major issue for the BBr_3 source for wurtzite phase BGaN was the incorporation of Br impurities. It is unknown if h-BN would have the same issue.

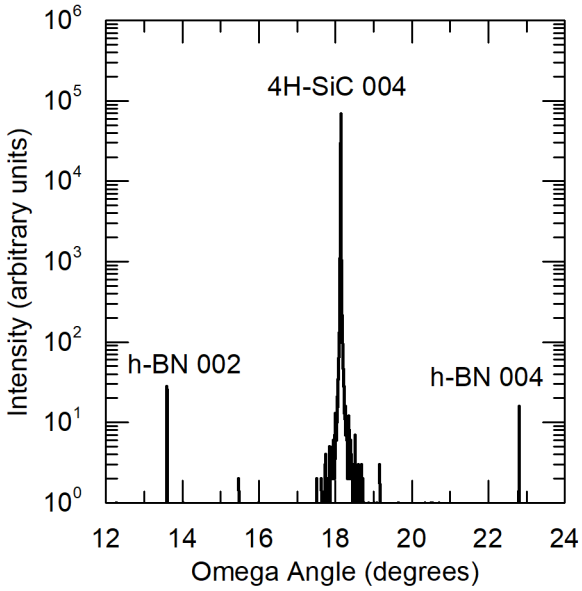

Figure 5.3 h-BN XRD
Large area omega two-theta scan around the 4H-SiC 0004 substrate peak. Signals at ~13.6° and ~22.9° are approximately where we would expect the peaks for h-BN 0002 and 0004 peaks respectively to be. The low Z ratio of both B and N means that BN has very low signal compared to SiC

References

[1] I. Vurgaftman, and J.R. Meyer, J. Appl. Phys. 94, 3675 (2003).

[2] R.C. Cramer, B. Bonef, J. English, C.E. Dreyer, C.G. Van de Walle, J. S. Speck, J. Vac. Sci. Technol. A 35, 041509 (2017)

[3] R. C. Cramer, B. Bonef, and J. S. Speck, *J. Vac. Sci. Technol. A* In Press (2019)

[4] X. Li, L. Tao, Z. Chen, H. Fang, X. Li, X. Wang, J. Xu, H. Zhu, Appl. Phys. Rev. 4, 021306 (2017) DOI: 10.1063/1.4983646

[5] C. Tan, X. Cao, X. Wu, Q. He, J. Yang, X. Zhang, J. Chen, W. Zhao, S. Han, G. Nam, M. Sindoro, and H. Zhang, Chem Rev. 117, 6225 (2017), DOI: 10.1021/acs.chemrev.6b00558

[6] D. Akinwande, C. J. Brennan, J. S. Bunch, P. Egberts, J. R. Felts, H. Gao, R. Huang, J. Kim, T. Li, Y. Li, K. M. Liechti, N. Lu, H. S. Park, E. J. Reed, P. Wang, B. I. Yakobson, T. Zhang, Y. Zhang, Y. Zhou, Y. Zhu, Extreme Mech. Lett. 13, 42 (2017) DOI: 10.1016/j.eml.2017.01.008

Chapter 6: Conclusions

A. Extreme III-nitrides

The extreme III-nitride alloys InAlN, BGaN, and BAlN all still have significant potential for future research. Due to complications caused by strain state and alloy quality the basic properties of these alloys as a function of composition are still difficult to reliably measure. Additionally there is much work to be done to find reliable growth techniques which produce both high crystal quality and low impurity concentration across all compositions.

InAlN is a well explored system yet still there is not a broad consensus on the functional form of the composition dependence of the bandgap. In Chapter 2 we presented data on the band gap of InAlN films with high In content which contributes to the set of band gap vs composition values available in the literature. The band gap data we present is ultimately derived from absorption data and we use a different fitting method than most of the literature. In our data analysis we interpolate the absorption data and perform numerical differentiation to determine the curvature of the data. We then define a region of low curvature as " linear " and perform our Tauc fit to that region. We expect this method to be more precise and reproducible than past methods of fitting "by eye". There is still significant work to be done in performing consistent accurate measurements of the band gap across the entire range and finding a functional form for the band bending which can be used to support a theoretical model.

In Chapters 3, 4, and 5 we demonstrated the growth of high crystal quality BGaN and BAlN films. This is a very new area of research and there is significant work yet to be done. We obtained good, random alloy, B incorporation in our BGaN films however our

composition was limited to 3.9% B on the group III site and we had extremely rough surface morphology. Exploring different growth modes for BGaN, particularly those at a higher temperature, may result in higher adatom mobility and a smoother surface. Additionally there is interest in determining the actual solubility limit of BN in wurtzite GaN. We are currently unsure if the clustering that we see of the B in films above 3.9% B on the group III site is due to phase separation or some other factor. Our work on BAlN is less complete than on BGaN leaving a great amount of research left to be done on the growth of BAlN using BBr_3 as a B source. Beyond structural quality the electrical and optical properties of the BGaN and BAlN films would be of great interest to the community.

B. Applications for BBr_3 in MBE

The BBr_3 source has been successful for incorporating B into group III nitrides. We have demonstrated good crystal quality random alloys of BGaN with B compositions up to 3.9% and our initial results for BAlN are similarly promising. However the BBr_3 source itself is a significant source of O, C, and Br impurities in the films.

The O and C incorporation in our BGaN films is most likely a result of the low purity source we used as a proof of concept. We expect with a higher purity source these contaminants would not be present. The Br incorporation from the source is more likely a fundamental limitation for the growth BGaN and BAlN using BBr_3. It is possible that in some drastically different growth regime the Br incorporation would fall to acceptable levels however this seems unlikely. Additionally while it is unknown what type of dopant Br would be in BGaN and BAlN it is likely electrically active which would severely limit any potential applications of Br doped material. This means that it is likely that BBr_3 is not going to be a good source for BGaN and BAlN. There is some potential for BBr_3 to be used as a B source in MBE growth of other materials such as h-BN which we have demonstrated a proof of concept.

Appendix A: Paired off-axis HRXRD

Using High Resolution X-Ray Diffraction (XRD) on wurtzite structure III-nitride films is a well-established method for determining film properties. The most common XRD measurement is the on-axis 0002 ω-2θ scan from which one can directly measure the c parameter of a film relative to the substrate and, if fringes are present, the thickness of the coherent region. In high crystal quality films the coherent region is the entirety of the film thickness.

Measuring the a parameter of films via XRD is more difficult due to the fact that in general XRD is aligned to the reflection condition of the substrate not the film. If the film and substrate have the same c/a ratio than an ω-2θ scan of an off axis scattering condition aligned to the substrate peak will correctly give the planar spacing for the given reflection and then the a parameter can be calculated using the measured d spacing of the off axis reflection and the c parameter measured from the on axis scan. However this is rarely the case if the c/a ratio of the film is not the same as that of the substrate than an off axis ω-2θ scan is insufficient.

To determine the a parameter of a film with an c/a ratio different from that of the substrate (which is almost always the case) the next technique employed is often the paired off axis ω measurement.[1] In this measurement scheme an open detector is used and an omega scan is performed around a pair of off axis substrate peaks 180° from each other (relative to a rotation about [0001] for a (0001) oriented layer) such as $10\bar{1}5$ and $\bar{1}015$. Using the separation in omega between the film and substrate peaks in these two geometries the a and c parameter can be determined as was described by Bauer and Richter.[1] A scale

schematic of diffraction vectors necessary to measure the $10\bar{1}5$ peaks of GaN and $In_{0.5}Al_{0.5}N$ are shown in Figure A.1.

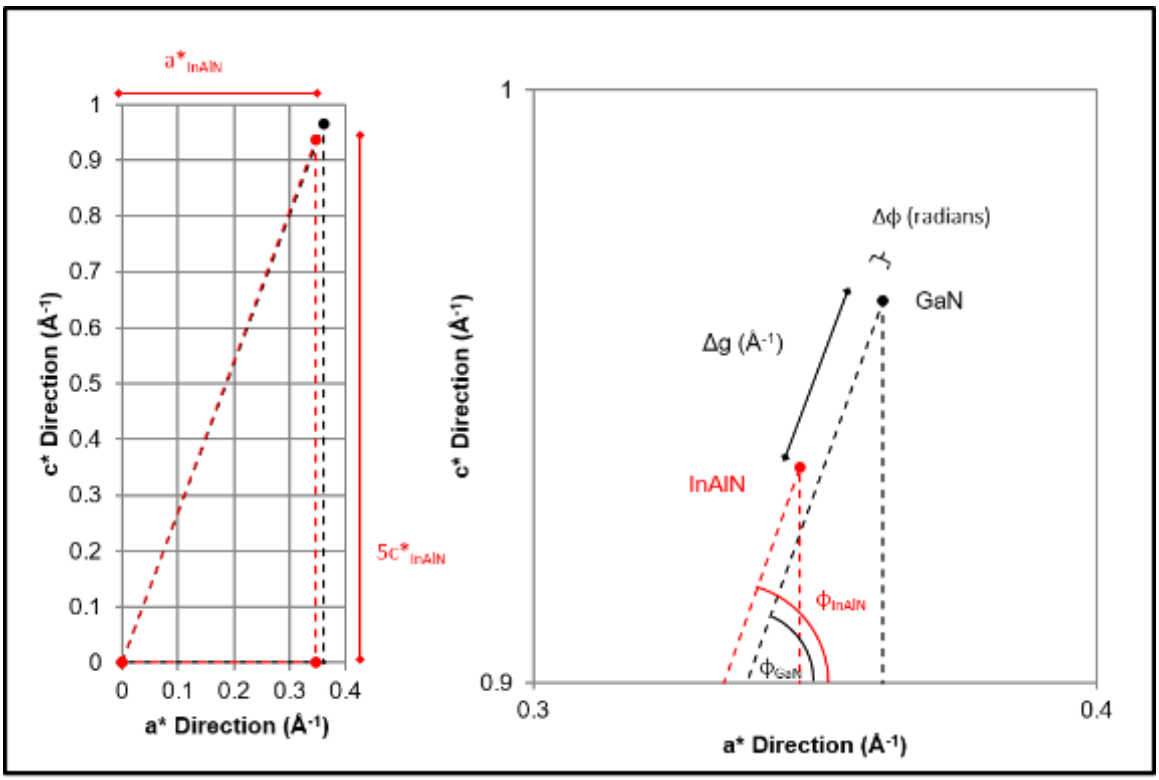

Figure A.1 Scale representation of $In_{0.5}Al_{0.5}N$ and GaN $10\bar{1}5$ peaks.
A to scale diagram showing the separation between the GaN substrate peak and an $In_{0.5}Al_{0.5}N$ film peak in reciprocal space.

In Figure A.1 the black triangle is defined by the crystal parameters of the GaN substrate and the conditions in reciprocal space that correspond to the $10\bar{1}5$ reflection. The width of the triangle is 1 x a^* ($a^* = 4\pi/a\sqrt{3}$), the height of the triangle is 5 x c^* ($c^* = 2\pi/c$) and the hypotenuse of the triangle is the g vector for the 1015 reflection which has a magnitude of $2\pi/d$ where d is the spacing for that reflection. The red triangle has comparable definitions using the parameters of $In_{0.5}Al_{0.5}N$ instead of GaN. Δg is the difference in the magnitude of the g vectors for GaN and $In_{0.5}Al_{0.5}N$ and φ is the angle between the g vector and the axis of

rotation. In an asymmetric scan omega and 2θ are both offset by φ. The definitions in Figure A.1 are consistent with those used by Bauer and Richter.[1]

In the course of the InAlN experiment described in Chapter 2 we initially tried to use the paired off axis technique to independently measure the a and c parameters of the InAlN films but found that it did not work across all compositions. We determined that the experiment was limited by the width of our open detector. To expand the range of the scan we performed the measurement with an ω-2θ geometry but with an open detector with the justification that this would effectively increase our detector width. Even with the technique it was determined that for InAlN the c/a parameter is sufficiently different that for a majority of compositions some or all of the off axis peak intensity falls outside of our scanning range as shown in Figure A.2.

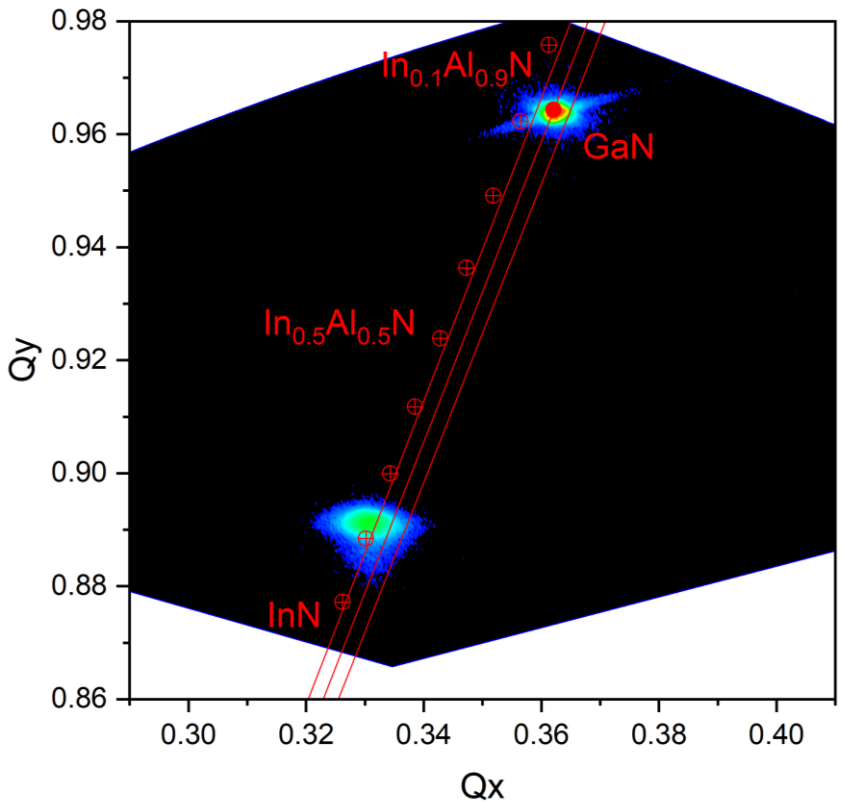

Figure A.2 Limits of an Open Detector ω-2θ scan.
(Filled circle) theoretical $10\bar{1}5$ GaN reflection, (crossed circles) theoretical $10\bar{1}5$ peaks for InAlN with In = 0, 0.1, 0.2, 0.3, 0.4, 0.5, 0.6, 0.7, 0.8, 0.9, and 1.0 (central arc) the arc of an ω-2θscan (side arcs) the edges of the detection region from an open detector ω-2θscan (background) real RSM data for the $In_{0.87}Al_{0.13}N$ sample discussed in chapter 2.

Due to this limitation we used reciprocal space maps to independently measure the a and c parameters of the films. In general reciprocal space maps are easier to use however they have lower special resolution than triple axis scans which lowers overall accuracy. The paired off axis measurement technique would work for such films if the open detector had a larger angular acceptance though at particularly large ω separation values the error will be more significant due to a small angle approximation in the derivation of the paired off axis measurement analysis.

Appendix A Reference

[1] G. Bauer, W. Richter, *Optical Characterization of Epitaxial Semiconductor* layers. Berlin, Heidelberg: Springer Berlin Heidelberg (1996) ISBN 3-540-59129-X

Appendix B: The BBr_3 source at UCSB

The novel BBr_3 source used to grow the extreme B containing nitrides discussed in chapters 3, 4, and 5 is described in general in the experimental section of Chapter 4. This appendix goes into further detail with pictures of the specific source at UCSB and may be of particular interest to future researchers learning to operate the BBr_3 cabinet at UCSB or those seeking to create a similar system.

When setting up the BBr_3 after a system opening or an extended period without use it is important to check that the following things are in place:

1. **Cooling Water Flow**. The thermoelectric that control the bubbler temperature are hooked up to the house cooling water via the standard cooling water manifold on the Gen II. Without the cooling water the thermoelectrics cannot lower the temperature.
2. **Compressed Air**. The valves in the BBr_3 cabinet are pneumatic. They need to be connected to the house compressed air source to have sufficient pressure to function. As of 2019 the house compressed nitrogen source provides insufficient pressure to fully operate the valves and the compressed air line must connect to the 100+ psi compressed air line.
3. **N_2 Safety Purge**. The BBr_3 bubbler is contained within an outer shell which is purged with nitrogen. The inlet needs to be connected to the house nitrogen line, the outlet vents into the room. This is a safety precaution to help mitigate the damage in the event of a leak. BBr_3 will react with water, including water vapor in the air, to form HBr which is corrosive and dangerous.

4. **Gas Line Heating**. BBr_3 is a liquid at room temperature to prevent condensation within the gas lines they are heated when the system is in use. This is accomplished by wrapping the tubing both within the cabinet and along the gas flow path in bake tape and powering it with a variac. Generally we heated to lines to just over 100 °C as measured by an infrared thermometer.
5. **Let the Bubbler Temperature Equilibrate.** The temperature on the thermoelectric readout is on the outside of the bubbler it can take a long time for the BBr_3 itself to equilibrate in temperature. After you change the set point temperature on the bubbler it can take up to an hour for the resultant flux to fully stabilize.

Additional Information which may be useful is a set of specific BBr_3 system conditions and the resultant BBr_3 fluxes as measured via the beam flux monitor (Table B.1). The most recent set of measured fluxes from 2019 were all performed using a fully open leak valve (3.8 V) and the orifice bypass valve closed. Note that the beam flux monitor values are qualitatively useful only for comparing to other beam flux values for the same species. 1×10^{-7} Torr of BBr_3 is not the same molecular flux as 1×10^{-7} Torr of Ga.

Table B.1 BBr_3 Cabinet Operation conditions 2019

BBr_3 Bubbler Temperature	Leak Valve	Bypass Position	BBr_3 Beam Equivalent Pressure
-10 °C	3.8 V	Closed	4.29×10^{-8} Torr
0 °C	3.8 V	Closed	1.13×10^{-7} Torr
10 °C	3.8 V	Closed	1.77×10^{-7} Torr
20 °C	3.8 V	Closed	3.60×10^{-7} Torr
27 °C	3.8 V	Closed	5.42×10^{-7} Torr

The rest of this appendix consists of labeled figures of the various parts of the BBr_3 injection system which may be helpful for future operators to orient themselves (Figures B.1 through B.6).

Figure B.1 Cabinet Valves

The top picture is the schematic and control unit located on the control rack. The bottom picture is the view inside the BBr_3 cabinet. (a.) Valve to BBr_3 bubbler (b.) Control valve, also controls bypass see Fig. A.2 (c.) Variable leak valve (see Fig A.3) (d.) Run valve (e.) Valve to MBE, see Fig. A.4 (f.) Roughing line pressure gauge (g.) Manual valve which can be connected to a roughing pump (h.) Valves to open manifold lines to the roughing lines. Unless actively roughing these should always be closed (i.) Valve to cabinet ion pump (j.) Key control. In start mode all switches operate independently, in operate mode the run and vent valves are controlled by (k.) The toggle valve. In the run position the run valve is opened and the vent valve is closed and vice versa for the vent position. In computer position all valves are controlled by the computer though that was not set up in 2019. (l.) On/off switch for the thermodynamic temperature controls, note the cooling water must be flowing to provide cooling in order for the thermodynamic controls to work (m.) Control unit for the thermodynamic controls which has a range of -20° C to 30° C.

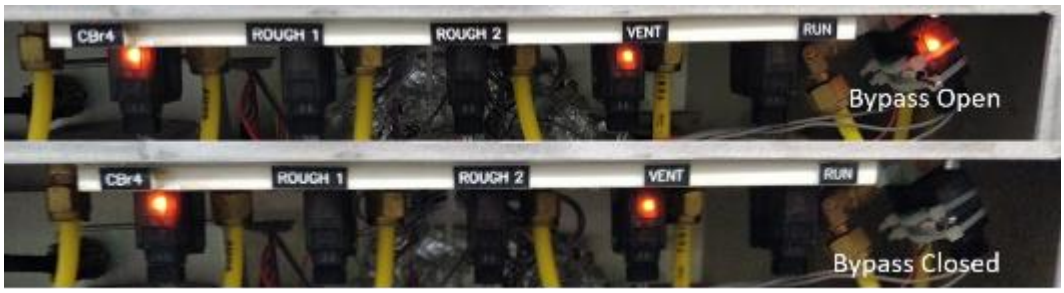

Figure B.2 Bypass Valve

Inside the BBr_3 cabinet there is a small switch on the top right side that controls the bypass valve. The bypass valve is interlocked with the BBr_3 valve (b in Figure B.1) it's labeled CBr_4 in the above picture since the cabinet is a repurposed experimental CBr_4 cabinet. If the bypass switch is down opening the BBr_3 valve will also open the bypass valve. If the switch is up the bypass will remain closed. The light will only turn on when the valve is actually open so only if both the bypass is in the down position and the BBr_3 valve is open.

Figure B.3 BBr_3 Control Units on the Cart
(a.) Temperature of the gas lines within the cabinet. (b.) Leak valve position as measured by a voltage 0.7 V is closed 3.8 V is fully open (c.) Manometer readout for the gas lines immediately above the BBr_3 bubbler. (d.) Ion pump control unit. (e.) On/off switches for the leak valve controller. (f.) Control switch to adjust the leak valve position.

Figure B.4 Gas line from BBr_3 cabinet to the MBE
(a.) Gas line from the BBr_3 cabinet to the MBE, the gas line is wrapped in bake tape and foil the temperature of the gas line can be controlled using the variac. (b.) T-valve between the BBr_3 line and the joined BBr_3/CBr_4 line (c.) Final valve between the gas lines and the MBE head-on injector.

Figure B.5 BBr_3 bubbler without nitrogen can
(a.) Bubbler manual valve. (b.) Outlet valve for N_2 purge (c.) Inlet for N_2 purge (d.) Cooling water in and out lines which provide a heat sink for the thermoelectric. (e.) Thermoelectric which can control the bubbler temperatures between -20° and 30° C.

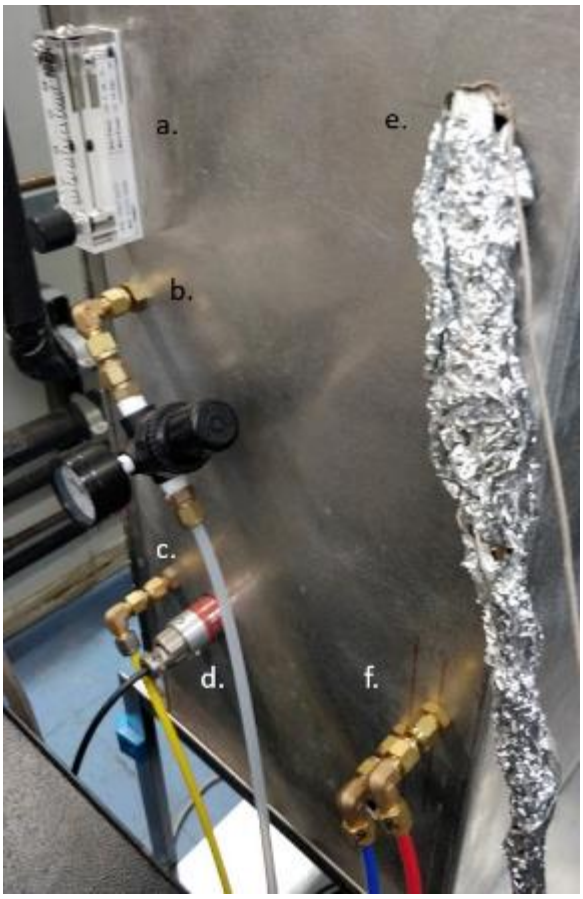

Figure B.6 Side of the BBr_3 Cabinet
(a.) N_2 purge line flow gauge (b.) N_2 purge line inlet (c.) Compressed air to operate pneumatic valves (d.) High voltage cord for the ion pump (e.) Outlet BBr_3 gas line to the MBE (f.) Cooling water supply (blue) and return (red) lines.